Geophysical Prospecting EAGE EUROPEAN ASSOCIATION OF GEOSCIENTISTS & ENGINEERS

Geophysical Prospecting, 2012, **60**, 802–823 doi: 10.1111/j.1365-2478.2012.01056.x

On the relation between seismic interferometry and the simultaneous-source method

Kees Wapenaar*, Joost van der Neut and Jan Thorbecke

Department of Geoscience and Engineering, Delft University of Technology, PO Box 5048, 2600 GA Delft, The Netherlands

Received July 2011, revision accepted October 2011

ABSTRACT

In seismic interferometry the response to a virtual source is created from responses to sequential transient or simultaneous noise sources. Most methods use crosscorrelation, but recently seismic interferometry by multidimensional deconvolution (MDD) has been proposed as well. In the simultaneous-source method (also known as blended acquisition), overlapping responses to sources with small time delays are recorded. The crosstalk that occurs in imaging of simultaneous-source data can be reduced by using phase-encoded sources or simultaneous noise sources, by randomizing the time interval between the shots, or by inverting the blending operator. Seismic interferometry and the simultaneous-source method are related. In this paper we make this relation explicit by deriving deblending as a form of seismic interferometry by MDD. Moreover, we discuss a deblending algorithm for blended data acquired at the surface.

1 INTRODUCTION

In seismic interferometry the response to a virtual source is created from responses to sequential transient sources (Schuster *et al.*, 2004; Bakulin and Calvert, 2006; Mehta *et al.*, 2007) or simultaneous noise sources (Shapiro and Campillo, 2004; Larose *et al.*, 2006; Draganov *et al.*, 2007; Gouédard *et al.*, 2008). Most methods use crosscorrelation, but recently seismic interferometry by multidimensional deconvolution (MDD) has been proposed as well (Wapenaar, Slob and Snieder, 2008; van der Neut *et al.*, 2011).

In the simultaneous-source method (also known as blended acquisition), overlapping responses to sources with small time delays are recorded (Beasley, Chambers and Jiang, 1998; Beasley, 2008). The crosstalk that occurs in imaging of simultaneous-source data can be reduced by using phase-encoded sources (Bagaini, 2006; Ikelle, 2007; Neelamani *et al.*, 2008; Herrmann, Erlangga and Lin, 2009; Schuster *et al.*, 2011) or simultaneous noise sources (Howe *et al.*, 2008), by randomizing the time interval between the shots (Stefani, Hampson and Herkenhoff, 2007; Hampson, Stefani and Herkenhoff, 2008) possibly followed by a noise filtering process (Akerberg *et al.*, 2008; Moore *et al.*, 2008; Huo, Luo and Kelamis, 2009), by prediction and subtraction (Spitz, Hampson and Pica, 2008; Kim *et al.*, 2009; Mahdad, Doulgeris and Blacquière, 2011), by inverting the blending operator using sparseness constraints (Berkhout, 2008; Abma *et al.*, 2010) or by integrating the deblending process with seismic migration (Romero *et al.*, 2000; Dai and Schuster, 2009; Tang and Biondi, 2009; Verschuur and Berkhout, 2011).

Seismic interferometry and the simultaneous-source method are related. In this paper we make this relation explicit by deriving deblending as a form of seismic interferometry by multidimensional deconvolution. The setup is as follows. In section 2 we review seismic interferometry by MDD. In section 3 we derive deblending by MDD as a form of seismic interferometry by MDD. The resulting algorithm combines redatuming (an essential aspect of seismic interferometry) with deblending. In section 4 we discuss the least-squares inversion aspects of deblending by MDD in more detail. In section 5 we compare our algorithm for combined redatuming and deblending with existing algorithms that apply deblending directly at the surface. We show that there are some essential differences and use this

*E-mail: C.P.A.Wapenaar@tudelft.nl

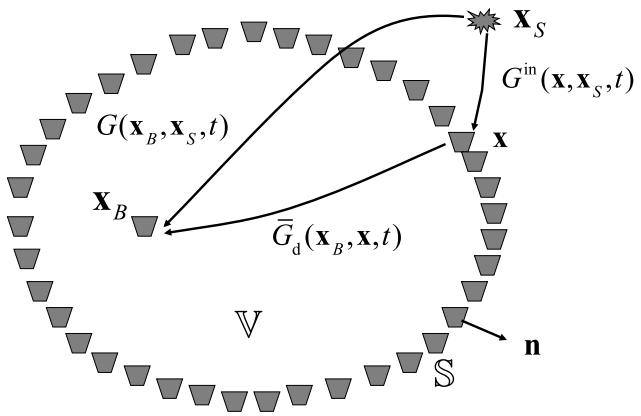

Figure 1 Configuration for the convolution-type Green's function representation (equation 1). The medium does not need to be lossless. The rays represent full responses, including primary and multiple scattering due to inhomogeneities inside as well as outside $\mathbb{S}$.

insight in the derivation of a deblending algorithm that operates directly on blended data at the surface.

2 SEISMIC INTERFEROMETRY BY MULTIDIMENSIONAL DECONVOLUTION

2.1 Convolution-type Green's function representation

We consider an arbitrary inhomogeneous acoustic medium, which may be either lossless or dissipative. In this medium we define a surface $\mathbb{S}$ with outward pointing normal vector $\mathbf{n}$, enclosing a volume $\mathbb{V}$ (Figure 1). Outside $\mathbb{V}$ there is a source located at $\mathbf{x}_S$ and inside $\mathbb{V}$ we consider a receiver at $\mathbf{x}_B$. The Green's function between this source and receiver is defined as $G(\mathbf{x}_B, \mathbf{x}_S, t)$, where t denotes time. For this configuration we consider the following convolutional Green's function representation (Wapenaar *et al.*, 2011)

$$G(\mathbf{x}_B, \mathbf{x}_S, t) = \oint_{\mathbb{S}} \bar{G}_{\text{d}}(\mathbf{x}_B, \mathbf{x}, t) * G^{\text{in}}(\mathbf{x}, \mathbf{x}_S, t)\, \text{d}\mathbf{x} \qquad (1)$$

(the asterisk ($*$) denotes temporal convolution). $G^{\text{in}}(\mathbf{x}, \mathbf{x}_S, t)$ is the part of the Green's function $G(\mathbf{x}, \mathbf{x}_S, t)$ that propagates inward into $\mathbb{V}$. $\bar{G}_{\text{d}}(\mathbf{x}_B, \mathbf{x}, t)$ is the response to a dipole source (indicated by the subscript 'd') at $\mathbf{x}$. It is related to the monopole response $\bar{G}(\mathbf{x}_B, \mathbf{x}, t)$ via

$$\rho\, \frac{\partial \bar{G}_{\text{d}}(\mathbf{x}_B, \mathbf{x}, t)}{\partial t} = -2\, \mathbf{n} \cdot \nabla \bar{G}(\mathbf{x}_B, \mathbf{x}, t). \qquad (2)$$

The bar denotes that $\bar{G}_{\text{d}}(\mathbf{x}_B, \mathbf{x}, t)$ is defined in a reference medium, which is identical to the actual medium in $\mathbb{V}$ and which is homogeneous outside $\mathbb{S}$, with mass density ρ and propagation velocity c (equivalently, $\mathbb{S}$ is an absorbing boundary for $\bar{G}_{\text{d}}(\mathbf{x}_B, \mathbf{x}, t)$). In the derivation of equation (1) it has been assumed that $\mathbb{S}$ is smooth and ρ is constant on $\mathbb{S}$. Apart from that, equation (1) involves no approximations.

We consider $\bar{G}_{\text{d}}(\mathbf{x}_B, \mathbf{x}, t)$ as the unknown quantity, hence equation (1) is an implicit representation of the convolution type for $\bar{G}_{\text{d}}(\mathbf{x}_B, \mathbf{x}, t)$. If it were a single equation, the inverse problem would be ill-posed. However, equation (1) holds for each source position $\mathbf{x}_S$ (outside $\mathbb{V}$), which we will denote from here onward by $\mathbf{x}_S^{(i)}$, where i denotes the source number. Solving the ensemble of equations for $\bar{G}_{\text{d}}(\mathbf{x}_B, \mathbf{x}, t)$ involves MDD, which will be discussed in more detail later. Because the bar denotes a reference situation, the retrieved Green's function $\bar{G}_{\text{d}}(\mathbf{x}_B, \mathbf{x}, t)$ is correct for the medium in $\mathbb{V}$ but it does not include scattering from inhomogeneities outside $\mathbb{S}$. This only improves the interpretability of the retrieved Green's function (assuming one is interested in the properties in $\mathbb{V}$ only). Note that the reference medium does not restrict the method, because the "measured" Green's functions G and G^{in} in equation (1) are defined in the actual medium.

Note that the integration in equation (1) takes place along $\mathbf{x}$, which is the receiver coordinate of the "measured" Green's functions $G^{\text{in}}(\mathbf{x}, \mathbf{x}_S^{(i)}, t)$. In most practical situations, receivers are not available on a closed boundary, so the integration in equation (1) is necessarily restricted to an open receiver boundary. As long as the source positions $\mathbf{x}_S^{(i)}$ are located at the appropriate side of $\mathbb{S}$ (i.e., outside $\mathbb{V}$), it suffices to take the integral over an (infinite) open receiver boundary (the integral over the remaining boundary vanishes because of Sommerfeld's radiation condition).

Equation (1) has been derived for the situation that $\mathbf{x}_B$ lies inside $\mathbb{V}$. In several applications $\mathbf{x}_B$ is a receiver on $\mathbb{S}$. For those applications we take $\mathbf{x}_B$ just inside $\mathbb{S}$ to avoid the complications of taking $\mathbf{x}_B$ on $\mathbb{S}$. Moreover, for those applications it is often useful to consider only the outward-propagating part of the field at $\mathbf{x}_B$. Applying decomposition at $\mathbf{x}_B$ at both sides of equation (1) gives

$$G^{\text{out}}(\mathbf{x}_B, \mathbf{x}_S^{(i)}, t) = \int_{\mathbb{S}} \bar{G}_{\text{d}}^{\text{out}}(\mathbf{x}_B, \mathbf{x}, t) * G^{\text{in}}(\mathbf{x}, \mathbf{x}_S^{(i)}, t)\, \text{d}\mathbf{x}. \qquad (3)$$

This equation is nearly the same (except for a different normalization) as our previously derived one-way representation for MDD (Wapenaar *et al.*, 2008).

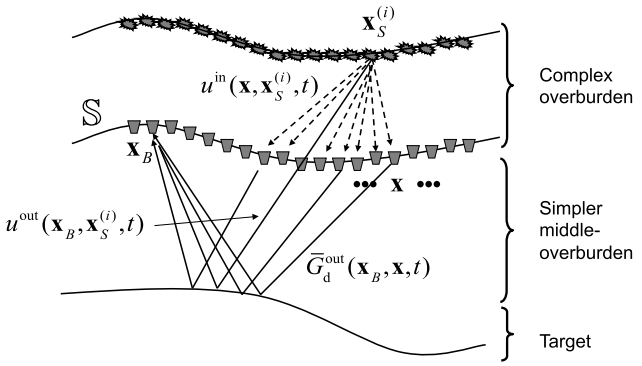

Figure 2 Modified configuration for the convolution-type Green's function representation. This configuration is the basis for data-driven redatuming by MDD.

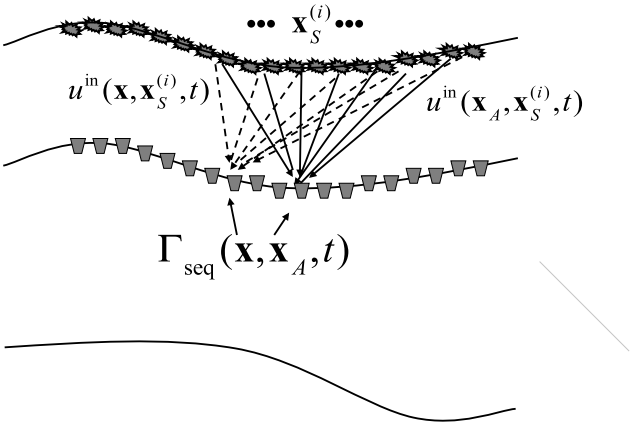

Figure 3 Illustration of the point-spread function $\Gamma_{\text{seq}}(\mathbf{x}, \mathbf{x}_A, t)$.

2.2 Sequential transient sources

For sequential transient sources we may write for the responses at $\mathbf{x}$ and $\mathbf{x}_B$

$$u^{\text{in}}(\mathbf{x}, \mathbf{x}_S^{(i)}, t) = G^{\text{in}}(\mathbf{x}, \mathbf{x}_S^{(i)}, t) * s^{(i)}(t - t_i), \tag{4}$$

$$u^{\text{out}}(\mathbf{x}_B, \mathbf{x}_S^{(i)}, t) = G^{\text{out}}(\mathbf{x}_B, \mathbf{x}_S^{(i)}, t) * s^{(i)}(t - t_i). \tag{5}$$

For the moment we assume that the "ignition times" t_i are sufficiently separated, so that the responses to different sources are not overlapping each other. We define the autocorrelation of the source signals as

$$s^{(i)}(t - t_i) * s^{(i)}(-t - t_i) = s^{(i)}(t) * s^{(i)}(-t) = S_{\text{seq}}^{(i)}(t). \tag{6}$$

By convolving both sides of equation (3) with $s^{(i)}(t - t_i)$ we obtain

$$u^{\text{out}}(\mathbf{x}_B, \mathbf{x}_S^{(i)}, t) = \int_{\mathbb{S}} \bar{G}_{\text{d}}^{\text{out}}(\mathbf{x}_B, \mathbf{x}, t) * u^{\text{in}}(\mathbf{x}, \mathbf{x}_S^{(i)}, t)\, \text{d}\mathbf{x}, \tag{7}$$

see Figure 2. Solving equation (7) in a least-squares sense is equivalent to solving its normal equation (Menke 1989; van der Neut *et al.*, 2010). We obtain the normal equation by crosscorrelating both sides of equation (7) with $u^{\text{in}}(\mathbf{x}_A, \mathbf{x}_S^{(i)}, t)$ (with $\mathbf{x}_A$ on $\mathbb{S}$) and taking the sum over all sources, according to

$$\sum_i u^{\text{out}}(\mathbf{x}_B, \mathbf{x}_S^{(i)}, t) * u^{\text{in}}(\mathbf{x}_A, \mathbf{x}_S^{(i)}, -t) = \int_{\mathbb{S}} \bar{G}_{\text{d}}^{\text{out}}(\mathbf{x}_B, \mathbf{x}, t) * \sum_i u^{\text{in}}(\mathbf{x}, \mathbf{x}_S^{(i)}, t) * u^{\text{in}}(\mathbf{x}_A, \mathbf{x}_S^{(i)}, -t)\, \text{d}\mathbf{x}. \tag{8}$$

We define the correlation function and the point-spread function for sequential transient-source responses as

$$C_{\text{seq}}(\mathbf{x}_B, \mathbf{x}_A, t) = \sum_i u^{\text{out}}(\mathbf{x}_B, \mathbf{x}_S^{(i)}, t) * u^{\text{in}}(\mathbf{x}_A, \mathbf{x}_S^{(i)}, -t) \tag{9}$$

and

$$\Gamma_{\text{seq}}(\mathbf{x}, \mathbf{x}_A, t) = \sum_i u^{\text{in}}(\mathbf{x}, \mathbf{x}_S^{(i)}, t) * u^{\text{in}}(\mathbf{x}_A, \mathbf{x}_S^{(i)}, -t), \tag{10}$$

respectively. With these definitions, we rewrite equation (8) as

$$C_{\text{seq}}(\mathbf{x}_B, \mathbf{x}_A, t) = \int_{\mathbb{S}} \bar{G}_{\text{d}}^{\text{out}}(\mathbf{x}_B, \mathbf{x}, t) * \Gamma_{\text{seq}}(\mathbf{x}, \mathbf{x}_A, t)\, \text{d}\mathbf{x}. \tag{11}$$

Equation (11) states that the correlation function $C_{\text{seq}}(\mathbf{x}_B, \mathbf{x}_A, t)$, defined by equation (9), is proportional to the Green's function $\bar{G}_{\text{d}}^{\text{out}}(\mathbf{x}_B, \mathbf{x}, t)$, with its source smeared in space and time by the point-spread function $\Gamma_{\text{seq}}(\mathbf{x}, \mathbf{x}_A, t)$. This point-spread function is defined, according to equation (10), as the crosscorrelation of the inward propagating fields at $\mathbf{x}_A$ and $\mathbf{x}$, summed over the source positions $\mathbf{x}_S^{(i)}$, see Figure 3. Under ideal circumstances the point-spread function approaches a temporally and spatially band-limited delta function (Wapenaar *et al.*, 2011, Appendix). Hence, under ideal circumstances the correlation function $C_{\text{seq}}(\mathbf{x}_B, \mathbf{x}_A, t)$ is a temporally and spatially band-limited version of the Green's function $\bar{G}_{\text{d}}^{\text{out}}(\mathbf{x}_B, \mathbf{x}, t)$. In more realistic situations the point-spread function can deviate significantly from a band-limited delta function, as we will see in sections 2.4, 3.2, etc. For a random medium, de Hoop *et al.* (2012) quantify the point-spread function in terms of the statistical parameters of the medium.

In order to retrieve the Green's function from the correlation function, the effect of the point-spread function needs to be removed by inverting equation (11). Because equation (11) represents a multidimensional convolution process along the

temporal and spatial axes[1], inversion of this equation is equivalent to multi-dimensional deconvolution (MDD). This will be further discussed in section 2.4.

2.3 Simultaneous noise sources

For simultaneous noise sources we write for the responses at $\mathbf{x}$ and $\mathbf{x}_B$

$$u^{\text{in}}(\mathbf{x}, t) = \sum_i G^{\text{in}}\left(\mathbf{x}, \mathbf{x}_S^{(i)}, t\right) * N^{(i)}(t), \tag{12}$$

$$u^{\text{out}}(\mathbf{x}_B, t) = \sum_i G^{\text{out}}\left(\mathbf{x}_B, \mathbf{x}_S^{(i)}, t\right) * N^{(i)}(t). \tag{13}$$

We define the crosscorrelation of the noise as

$$\langle N^{(i)}(t) * N^{(j)}(-t)\rangle = S^{(ij)}_{\text{noise}}(t), \tag{14}$$

where $S^{ij}_{\text{noise}}(t)$ represents the spatial (ij) and temporal (t) correlation function (we consider uncorrelated sources as a special case in Appendix A). Furthermore, $\langle\ \cdot\ \rangle$ denotes ensemble averaging. In practice, the ensemble averaging is replaced by integrating over sufficiently long time.

By convolving both sides of equation (3) with $N^{(i)}(t)$ and summing over i we obtain

$$u^{\text{out}}(\mathbf{x}_B, t) = \int_{\mathbb{S}} \bar{G}^{\text{out}}_{\text{d}}(\mathbf{x}_B, \mathbf{x}, t) * u^{\text{in}}(\mathbf{x}, t)\, \mathrm{d}\mathbf{x}. \tag{15}$$

Crosscorrelating both sides with $u^{\text{in}}(\mathbf{x}_A, t)$ (with $\mathbf{x}_A$ on $\mathbb{S}$) and averaging over time gives

$$\begin{aligned}&\left\langle u^{\text{out}}(\mathbf{x}_B, t) * u^{\text{in}}(\mathbf{x}_A, -t)\right\rangle \\ &\quad = \int_{\mathbb{S}} \bar{G}^{\text{out}}_{\text{d}}(\mathbf{x}_B, \mathbf{x}, t) * \langle u^{\text{in}}(\mathbf{x}, t) * u^{\text{in}}(\mathbf{x}_A, -t)\rangle\, \mathrm{d}\mathbf{x}.\end{aligned} \tag{16}$$

We define the correlation function and the point-spread function for noise source responses as

$$C_{\text{noise}}(\mathbf{x}_B, \mathbf{x}_A, t) = \langle u^{\text{out}}(\mathbf{x}_B, t) * u^{\text{in}}(\mathbf{x}_A, -t)\rangle \tag{17}$$

and

$$\Gamma_{\text{noise}}(\mathbf{x}, \mathbf{x}_A, t) = \langle u^{\text{in}}(\mathbf{x}, t) * u^{\text{in}}(\mathbf{x}_A, -t)\rangle, \tag{18}$$

respectively. With these definitions, we rewrite equation (16) as

$$C_{\text{noise}}(\mathbf{x}_B, \mathbf{x}_A, t) = \int_{\mathbb{S}} \bar{G}^{\text{out}}_{\text{d}}(\mathbf{x}_B, \mathbf{x}, t) * \Gamma_{\text{noise}}(\mathbf{x}, \mathbf{x}_A, t)\ \mathrm{d}\mathbf{x}. \tag{19}$$

This equation has the same form as equation (11) for sequential transient sources. A more detailed comparison of the correlation and point-spread functions appearing in equations (11) and (19) is presented in Appendix A.

2.4 Interferometric redatuming by multi-dimensional deconvolution

As an application of interferometry by multidimensional deconvolution, we consider the situation of data-driven redatuming, because this will provide a natural link with the simultaneous-source method, discussed in section 3. Figure 2 shows the configuration. Receivers are situated in a near-horizontal well, below a complex overburden. They record the responses to sources at $\mathbf{x}_S^{(i)}$ at the surface. The aim is to redatum the sources of the field $u^{\text{out}}(\mathbf{x}_B, \mathbf{x}_S^{(i)}, t)$ from the acquisition surface to the well in the subsurface, by using the measured response $u^{\text{in}}(\mathbf{x}, \mathbf{x}_S^{(i)}, t)$ as the redatuming operator, hence the name "data-driven redatuming" or "interferometric redatuming" (Schuster and Zhou 2006). Because this measured redatuming operator accounts for all complexities of the overburden between the surface and the well, the redatumed response is expected to be significantly simpler than the original response $u^{\text{out}}(\mathbf{x}_B, \mathbf{x}_S^{(i)}, t)$, particularly when the middle-overburden between the well and the target is simpler than the overburden above the well (Bakulin and Calvert 2004, 2006).

We illustrate the method of data-driven redatuming by MDD with a numerical example. Figure 4a shows the configuration: 128 sources, indicated by the red stars, are regularly distributed along the surface, with a lateral spacing of $\Delta_s =$ 15 m. These sources emit Ricker wavelets with a central frequency of 23 Hz. The modeling is done without free-surface effects. The responses are recorded by equidistantly spaced receivers ($\Delta_r = 15$ m), indicated by the black triangles, in a horizontal borehole at a depth of 200 m. The medium consists of a complex overburden with strong vertical and lateral variations between the acquisition surface and the borehole, a synclinal structure below the borehole and a target interface with a pinchout at a depth of 1200 m. Figure 4b shows the directly modeled response to a source at the central position of the receiver array. This response serves as a reference for data-driven redatuming.

First we evaluate the correlation function $C_{\text{seq}}(\mathbf{x}_B, \mathbf{x}_A, t)$, defined by equation (9). To this end we crosscorrelate $u^{\text{in}}(\mathbf{x}_A, \mathbf{x}_S^{(i)}, t)$ for fixed $\mathbf{x}_A$ (the central receiver) with $u^{\text{out}}(\mathbf{x}_B, \mathbf{x}_S^{(i)}, t)$ for all $\mathbf{x}_B$ along the borehole. We repeat this for all source positions $\mathbf{x}_S^{(i)}$ and sum the correlation results over the sources (equation 9). The result, shown in Figure 4c,

[1] The terminology "spatial convolution" is loosely used to denote the integral along $\mathbb{S}$. For a laterally invariant medium and a horizontal surface $\mathbb{S}$ it would be a true spatial convolution because in that case the point-spread function $\Gamma_{\text{seq}}(\mathbf{x}, \mathbf{x}_A, t)$ would depend only on the distance between $\mathbf{x}$ and $\mathbf{x}_A$ (and on time t, of course). For a laterally varying medium it would be more accurate to speak of a space-variant spatial convolution, but for convenience we simply call it (spatial) convolution.

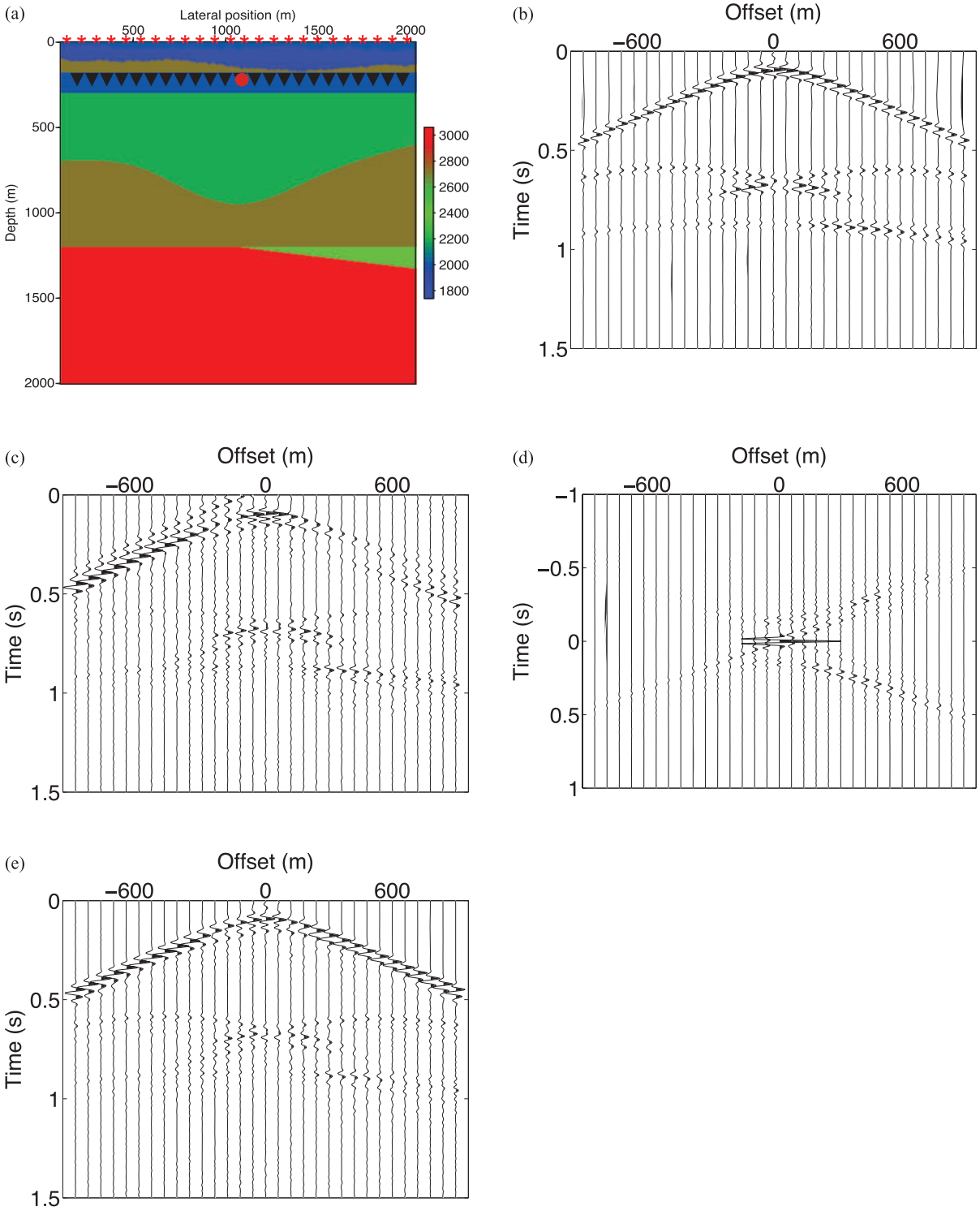

Figure 4 Numerical example of data-driven redatuming by multidimensional deconvolution. (a) Inhomogeneous medium configuration. The sources are situated at the surface (red stars) and the receivers in a horizontal borehole (the black triangles at a depth of 200 m) below a complex overburden. (b) Response to a source at the center of the receiver array, indicated by the red dot in (a). This response serves as a reference for the redatumed data in Figures 4c and 4e. (c) Correlation function. (d) Point-spread function. (e) Result of data-driven redatuming by MDD. (Figures (b) – (e) show every fourth trace.)

is an approximation of the response to a virtual source at $\mathbf{x}_A$ (the central receiver in the borehole, indicated by the red dot in Figure 4a), observed by all receivers $\mathbf{x}_B$ in the borehole (Bakulin and Calvert 2004, 2006; Mehta *et al.*, 2007). If we compare this correlation function with the reference response in Figure 4b, we see indeed that the main events are present, but there are also spurious events in the correlation function and the amplitudes are distorted.

The relation between the reference response and the correlation function is quantified by equation (11). The right-hand side of this equation states that the source of the Green's function (the reference response) is smeared in space and time by the point-spread function $\Gamma_{\text{seq}}(\mathbf{x}, \mathbf{x}_A, t)$. For the configuration of Figure 4a, the point-spread function is obtained, according to equation (10), by crosscorrelating the inward (downward) propagating fields at $\mathbf{x}_A$ and $\mathbf{x}$, and summing over the sources at the surface. It is shown in Figure 4d for fixed $\mathbf{x}_A$ and variable $\mathbf{x}$. Note that for the inversion of equation (11) it is required that point-spread functions like the one in Figure 4d are evaluated for all positions $\mathbf{x}_A$ along the borehole.

For the actual inversion we transform equation (11) from the time domain to the frequency domain and discretize the integral, according to

$$\hat{C}_{\text{seq}}\left(\mathbf{x}_B^{(k)}, \mathbf{x}_A^{(m)}, \omega\right) = \Delta_r \sum_l \hat{\bar{G}}_{\text{d}}^{\text{out}}\left(\mathbf{x}_B^{(k)}, \mathbf{x}^{(l)}, \omega\right) \hat{\Gamma}_{\text{seq}}(\mathbf{x}^{(l)}, \mathbf{x}_A^{(m)}, \omega), \tag{20}$$

where ω denotes the angular frequency and the circumflex denotes the frequency domain.The system of equations (20) can be solved for each frequency component separately. In practice this is done by a matrix inversion per frequency component. Because the point-spread function is temporally and spatially band-limited, this matrix inversion must be stabilized, see van der Neut *et al.* (2011). Transforming the end-result back to the time domain gives a band-limited estimate of $\bar{G}_{\text{d}}^{\text{out}}(\mathbf{x}_B^{(k)}, \mathbf{x}^{(l)}, t)$, which completes the MDD process. The result is shown in Figure 4e for fixed $\mathbf{x}^{(l)}$ and variable $\mathbf{x}_B^{(k)}$. Note that the match with the reference response (Figure 4b) is very good.

3 DEBLENDING BY MULTIDIMENSIONAL DECONVOLUTION

3.1 Convolutional model for the simultaneous-source method

Our starting point for the derivation of the convolutional model for the simultaneous-source method is the convolution-type Green's function representation (equation 3), which is repeated here for convenience

$$G^{\text{out}}\left(\mathbf{x}_B, \mathbf{x}_S^{(i)}, t\right) = \int_{\mathbb{S}} \bar{G}_{\text{d}}^{\text{out}}(\mathbf{x}_B, \mathbf{x}, t) * G^{\text{in}}(\mathbf{x}, \mathbf{x}_S^{(i)}, t)\, \text{d}\mathbf{x}. \tag{21}$$

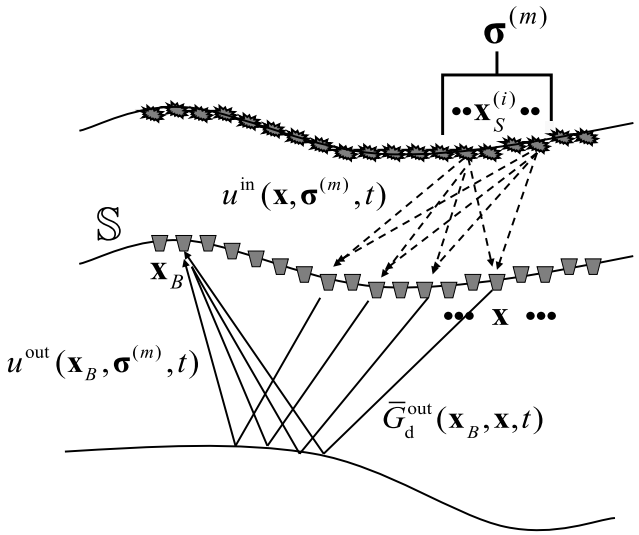

Figure 5 Convolutional model for the simultaneous-source method. This configuration is the basis for deblending by MDD.

Consider the configuration depicted in Figure 5, where $\boldsymbol{\sigma}^{(m)}$ denotes a group of source positions $\mathbf{x}_S^{(i)}$. The sources within a group emit delayed source wavelets $s^{(i)}(t - t_i)$, with ignition times t_i closely following one after another, so that the responses are measured with overlap. This is called "blended acquisition". We will assume that the ignition times of sources in different groups are sufficiently separated, so that the responses to different source groups can be measured without overlap. For source group $\boldsymbol{\sigma}^{(m)}$, the simultaneous-source responses at $\mathbb{S}$ are given by

$$u^{\text{in}}(\mathbf{x}, \boldsymbol{\sigma}^{(m)}, t) = \sum_{\mathbf{x}_S^{(i)} \in \boldsymbol{\sigma}^{(m)}} G^{\text{in}}\left(\mathbf{x}, \mathbf{x}_S^{(i)}, t\right) * s^{(i)}(t - t_i), \tag{22}$$

$$u^{\text{out}}(\mathbf{x}_B, \boldsymbol{\sigma}^{(m)}, t) = \sum_{\mathbf{x}_S^{(i)} \in \boldsymbol{\sigma}^{(m)}} G^{\text{out}}\left(\mathbf{x}_B, \mathbf{x}_S^{(i)}, t\right) * s^{(i)}(t - t_i), \tag{23}$$

where $\mathbf{x}_S^{(i)} \in \boldsymbol{\sigma}^{(m)}$ denotes that the summation takes place over all source positions $\mathbf{x}_S^{(i)}$ in group $\boldsymbol{\sigma}^{(m)}$. We define the crosscorrelation of the source signals as

$$s^{(i)}(t - t_i) * s^{(j)}(-t - t_j) = S_{\text{sim}}^{(ij)}(t - t_i + t_j) \tag{24}$$

(subscript "sim" stands for simultaneous). By convolving both sides of equation (21) with $s^{(i)}(t - t_i)$ and summing over all

sources in $\boldsymbol{\sigma}^{(m)}$ we obtain, analogous to equation (7),

$$u^{\text{out}}(\mathbf{x}_B, \boldsymbol{\sigma}^{(m)}, t) = \int_{\mathbb{S}} \bar{G}_{\text{d}}^{\text{out}}(\mathbf{x}_B, \mathbf{x}, t) * u^{\text{in}}(\mathbf{x}, \boldsymbol{\sigma}^{(m)}, t)\, \text{d}\mathbf{x}. \tag{25}$$

We obtain the normal equation by crosscorrelating both sides of equation (25) with $u^{\text{in}}(\mathbf{x}_A, \boldsymbol{\sigma}^{(m)}, t)$ (with $\mathbf{x}_A$ on $\mathbb{S}$) and taking the sum over all source groups $\boldsymbol{\sigma}^{(m)}$, according to

$$\sum_m u^{\text{out}}(\mathbf{x}_B, \boldsymbol{\sigma}^{(m)}, t) * u^{\text{in}}(\mathbf{x}_A, \boldsymbol{\sigma}^{(m)}, -t) = \int_{\mathbb{S}} \bar{G}_{\text{d}}^{\text{out}}(\mathbf{x}_B, \mathbf{x}, t) * \sum_m u^{\text{in}}(\mathbf{x}, \boldsymbol{\sigma}^{(m)}, t) * u^{\text{in}}(\mathbf{x}_A, \boldsymbol{\sigma}^{(m)}, -t)\, \text{d}\mathbf{x}. \tag{26}$$

We define the correlation function and the point-spread function for the simultaneous-source responses as

$$C_{\text{sim}}(\mathbf{x}_B, \mathbf{x}_A, t) = \sum_m u^{\text{out}}(\mathbf{x}_B, \boldsymbol{\sigma}^{(m)}, t) * u^{\text{in}}(\mathbf{x}_A, \boldsymbol{\sigma}^{(m)}, -t) \tag{27}$$

and

$$\Gamma_{\text{sim}}(\mathbf{x}, \mathbf{x}_A, t) = \sum_m u^{\text{in}}(\mathbf{x}, \boldsymbol{\sigma}^{(m)}, t) * u^{\text{in}}(\mathbf{x}_A, \boldsymbol{\sigma}^{(m)}, -t), \tag{28}$$

respectively. With these definitions, we rewrite equation (26) as

$$C_{\text{sim}}(\mathbf{x}_B, \mathbf{x}_A, t) = \int_{\mathbb{S}} \bar{G}_{\text{d}}^{\text{out}}(\mathbf{x}_B, \mathbf{x}, t) * \Gamma_{\text{sim}}(\mathbf{x}, \mathbf{x}_A, t)\, \text{d}\mathbf{x}. \tag{29}$$

This equation has the same form as equation (11) for sequential transient sources and equation (19) for simultaneous noise sources. A more detailed comparison of the correlation and point-spread functions appearing in equations (11), (19) and (29) is presented in Appendix A. Equations (A8) – (A11) describe the correlation function and point-spread function for blended acquisition. The terms denoted as "crosstalk" account for all crosscorrelations of responses to different sources within a group, summed over the groups. They are proportional to the crosscorrelations $S_{\text{sim}}^{(ij)}(t - t_i + t_j)$, defined in equation (24). For phase-encoded sources (Bagaini, 2006; Ikelle, 2007; Neelamani *et al.*, 2008, Herrmann *et al.*, 2009; Schuster *et al.*, 2011) or uncorrelated noise signals (Howe *et al.*, 2008) these crosscorrelations for $i \neq j$ are small. On the other hand, when the ignition times t_i are randomized, the crosscorrelations $S_{\text{sim}}^{(ij)}(t - t_i + t_j)$ for $i \neq j$ do not add coherently, which also helps to reduce the crosstalk (Stefani *et al.*, 2007; Hampson *et al.*, 2008). For those cases the correlation function $C_{\text{sim}}(\mathbf{x}_B, \mathbf{x}_A, t)$ is a reasonable approximation of the unblended response $\bar{G}_{\text{d}}^{\text{out}}(\mathbf{x}_B, \mathbf{x}_A, t) * S_{\text{sim}}^{(ii)}(t)$. For other situations, in which the crosstalk is not small, the unblended virtual-source response $\bar{G}_{\text{d}}^{\text{out}}(\mathbf{x}_B, \mathbf{x}, t)$ can be obtained from the blended data by inverting equation (29) by MDD. This is the subject of the next section.

3.2 Deblending by multi-dimensional deconvolution

In section 2.4 we discussed interferometry as a form of data-driven redatuming, which brings the sources of the fields $u^{\text{out}}(\mathbf{x}_B, \mathbf{x}_S^{(i)}, t)$ from the acquisition surface to the receiver positions in the horizontal borehole, using the response $u^{\text{in}}(\mathbf{x}, \mathbf{x}_S^{(i)}, t)$ as a measured redatuming operator. In a similar way we could redatum the sources of the blended fields $u^{\text{out}}(\mathbf{x}_B, \boldsymbol{\sigma}^{(m)}, t)$ from the surface to the borehole, using $u^{\text{in}}(\mathbf{x}, \boldsymbol{\sigma}^{(m)}, t)$ as the measured operator. Ideally this would give the deblended response $\bar{G}_{\text{d}}^{\text{out}}(\mathbf{x}_B, \mathbf{x}, t)$ for any virtual-source position $\mathbf{x}$ in the borehole, hence, with this procedure we would combine data-driven redatuming with source deblending. Of course this would require the availability of data acquired with receivers in a borehole. However, simultaneous-source acquisition is usually done with sources and receivers at the surface. For this more common situation we combine more traditional model-driven redatuming with source deblending. For this situation we do not aim to remove complex overburden effects, like in section 2.4, but the main purpose is to apply source deblending with similar algorithms as developed for seismic interferometry by MDD (in section 5 we discuss a related deblending-by-MDD method which circumvents the redatuming step altogether and leads to deblended data with sources and receivers at the surface).

For combined model-driven redatuming and source-deblending we assume that a macro model of the overburden, through which the redatuming will take place, is available. Using this macro model, the receivers of the blended data are downward extrapolated from the surface to a datum $\mathbb{S}$ in the subsurface, giving $u^{\text{out}}(\mathbf{x}_B, \boldsymbol{\sigma}^{(m)}, t)$. Moreover, the source groups are downward extrapolated to the same datum, giving $u^{\text{in}}(\mathbf{x}, \boldsymbol{\sigma}^{(m)}, t)$.

From here onward we assume that $u^{\text{in}}(\mathbf{x}, \boldsymbol{\sigma}^{(m)}, t)$ and $u^{\text{out}}(\mathbf{x}_B, \boldsymbol{\sigma}^{(m)}, t)$ are available and we leave undetermined whether these fields are decomposed blended wave fields measured in the borehole, or downward extrapolated blended data and source groups, originally acquired at the surface. We illustrate with a numerical example how we obtain the deblended virtual-source response $\bar{G}_{\text{d}}^{\text{out}}(\mathbf{x}_B, \mathbf{x}, t)$ from these blended fields. Consider the configuration in Figure 6a. There are 128 sources, indicated by the red stars, regularly distributed along the surface, with a lateral spacing of $\Delta_s = 15$ m. The sources emit Ricker wavelets with a central frequency of 23 Hz. The black triangles at a depth of 200 m represent equidistantly spaced receivers ($\Delta_r = 15$ m) at which the fields u^{in} and u^{out} are measured or to which they have been downward extrapolated. Because in this example the emphasis is

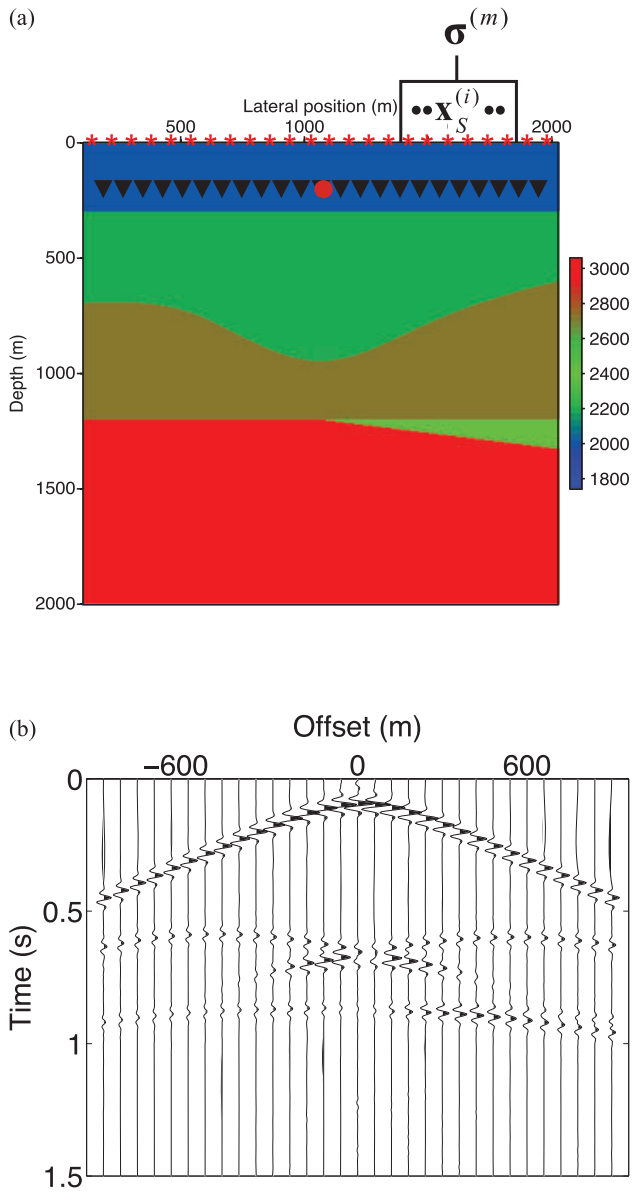

Figure 6 Numerical example of deblending by MDD. (a) Inhomogeneous medium configuration. The sources are situated at the surface (red stars, source interval $\Delta_s = 15$ m) and the receivers in the subsurface at a depth of 200 m (black triangles, receiver interval $\Delta_r = 15$ m). The data are blended by forming 32 source groups $\boldsymbol{\sigma}^{(m)}$ of four adjacent sources. (b) Directly modeled response to a source at the position of the red dot in (a). This response (which shows every fourth trace) serves as a reference for the deblended data in Figures 7d, 8d, 10d, 11d and 12d.

on deblending, the medium between the sources and receivers consists of a simple homogeneous layer with a propagation velocity of 2000 m/s. Below the receivers the medium is inhomogeneous in the lateral as well as in the vertical direction. The red dot denotes the position of the virtual source for which we will evaluate the redatumed deblended responses. Figure 6b shows a directly modeled response to a source at the position of the red dot. This response will serve as a reference.

First we consider the situation of regular blending. We form 32 source groups $\boldsymbol{\sigma}^{(m)}$, each containing four adjacent sources which emit transient wavelets, 0.25 s after one another. The blended data $u^{\text{out}}(\mathbf{x}_B, \boldsymbol{\sigma}^{(m)}, t)$ are shown in Figure 7a for a source group $\boldsymbol{\sigma}^{(m)}$ at the center of the acquisition surface. We crosscorrelate $u^{\text{in}}(\mathbf{x}_A, \boldsymbol{\sigma}^{(m)}, t)$ for fixed $\mathbf{x}_A$ (the red dot) with $u^{\text{out}}(\mathbf{x}_B, \boldsymbol{\sigma}^{(m)}, t)$ for all $\mathbf{x}_B$ along the receiver array. We repeat this for all source groups $\boldsymbol{\sigma}^{(m)}$ and sum the individual correlation results obtained for the different source groups (equation 27). The resulting correlation function $C_{\text{sim}}(\mathbf{x}_B, \mathbf{x}_A, t)$ is shown in Figure 7b for fixed $\mathbf{x}_A$ and variable $\mathbf{x}_B$. In this figure we recognize the reference response of Figure 6b as well as significant crosstalk, conform equations (A8) and (A10). Because this correlation function contains the correct response, results like this are sometimes called "pseudo-deblended data" (Berkhout 2008; Mahdad *et al.*, 2011). Next the point-spread function is computed by crosscorrelating the downward propagating fields u^{in} at the receiver array and summing over the source groups (equation 28). The result $\Gamma_{\text{sim}}(\mathbf{x}, \mathbf{x}_A, t)$ for fixed $\mathbf{x}_A$ and variable $\mathbf{x}$ is shown in Figure 7c. It exhibits a temporally and spatially band-limited delta function at zero time and zero offset, as well as crosstalk, conform equations (A9) and (A11). According to equation (29), the correlation function in Figure 7b is proportional to the Green's function $\bar{G}_{\text{d}}^{\text{out}}(\mathbf{x}_B, \mathbf{x}, t)$, with its source temporally and spatially convolved with the point-spread function of Figure 7c. In other words, the crosstalk in the point-spread function explains the crosstalk in the correlation function. The Green's function $\bar{G}_{\text{d}}^{\text{out}}(\mathbf{x}_B, \mathbf{x}, t)$ can be resolved by inverting equation (29). This inversion is a multidimensional deconvolution (MDD) process. Analogous to the inversion of equation (11) for interferometric redatuming, we implement deblending by MDD as a least-squares inversion (the details are discussed in section 4). The deblending result is shown in Figure 7d. Note that the crosstalk has been largely suppressed and that the remaining events accurately match the reference response in Figure 6b.

Next we consider the situation of irregular blending. We form again 32 source groups $\boldsymbol{\sigma}^{(m)}$, each containing four adjacent sources which emit transient wavelets, but this time the ignition times within one source group are chosen randomly from a uniform distribution between 0 and 1 s. Figures 8a, 8b and 8c show the blended data, the correlation function and the point-spread function, respectively. Obviously the crosstalk

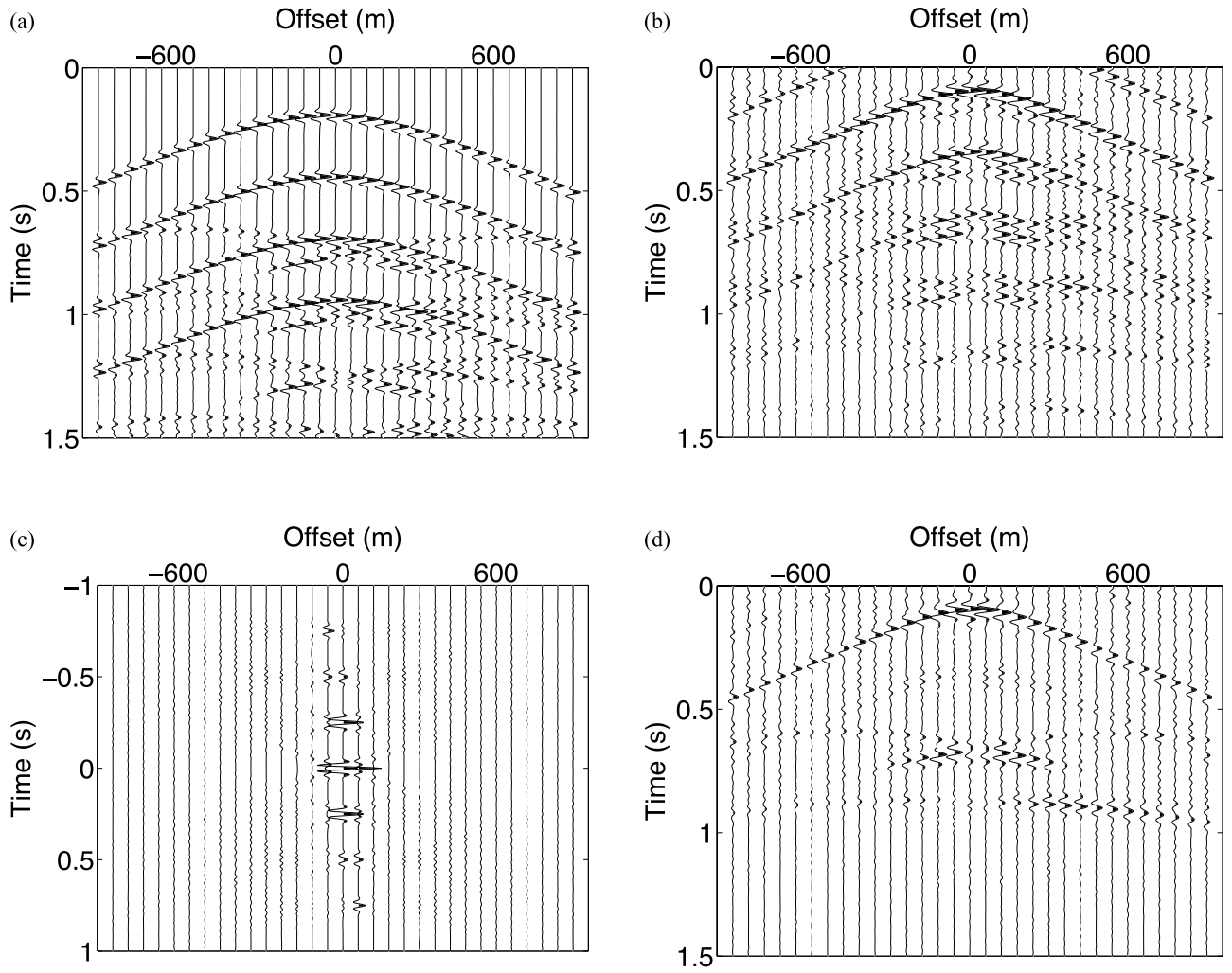

Figure 7 Results for regularly blended data (the time interval between the sources in a group equals 0.25 s). (a) Blended data $u^{\text{out}}(\mathbf{x}_B, \boldsymbol{\sigma}^{(m)}, t)$ for a source group $\boldsymbol{\sigma}^{(m)}$ at the center of the acquisition surface. (b) Correlation function $C_{\text{sim}}(\mathbf{x}_B, \mathbf{x}_A, t)$ (also known as pseudo-deblended data). (c) Point-spread function $\Gamma_{\text{sim}}(\mathbf{x}, \mathbf{x}_A, t)$. (d) Result of deblending by MDD. (These figures show every fourth trace.)

is much more dispersed than in Figures 7b and 7c. The deblended result in Figure 8d again accurately matches the reference response in Figure 6b. The result is somewhat better than in Figure 7d, probably because the notches in the spectrum of the point-spread function in Figure 8c are less severe than those in the spectrum of Figure 7c.

4 DISCUSSION OF LEAST-SQUARES INVERSION ASPECTS OF DEBLENDING BY MULTI-DIMENSIONAL DECONVOLUTION

In section 2.2 we introduced interferometric redatuming by MDD as a form of least-squares inversion. In section 3.2 we showed that deblending by MDD is also implemented as a least-squares inversion. Here we discuss the least-squares inversion aspects of deblending by MDD in more detail.

4.1 Convolutional model in matrix notation

We start by reformulating the convolutional model of section 3.1 into matrix notation (Berkhout 1982). Transforming equation (21) to the frequency domain and discretizing the integral gives

$$\hat{G}^{\text{out}}(\mathbf{x}_B^{(k)}, \mathbf{x}_S^{(i)}, \omega) = \Delta_r \sum_l \hat{\tilde{G}}_{\text{d}}^{\text{out}}(\mathbf{x}_B^{(k)}, \mathbf{x}^{(l)}, \omega)\hat{G}^{\text{in}}(\mathbf{x}^{(l)}, \mathbf{x}_S^{(i)}, \omega). \tag{30}$$

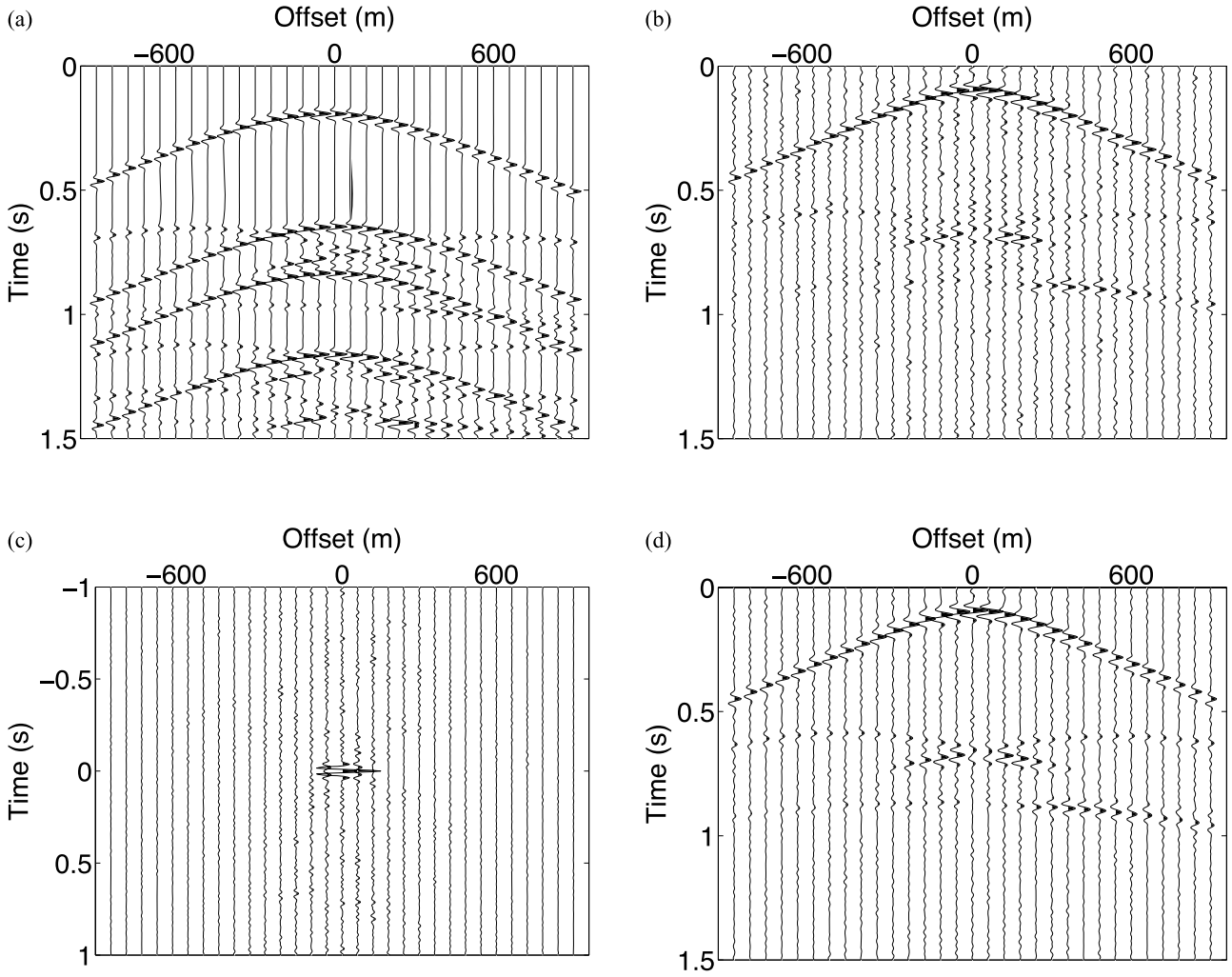

Figure 8 As in Figure 7, but for irregularly blended data (random ignition times).

For each frequency component this expression can be written as

$$\mathbf{G}^{\text{out}} = \tilde{\mathbf{G}}_{\text{d}}^{\text{out}}\mathbf{G}^{\text{in}}, \tag{31}$$

where the element at the lth row and ith column of matrix $\mathbf{G}^{\text{in}}$ contains $\hat{G}^{\text{in}}(\mathbf{x}^{(l)}, \mathbf{x}_S^{(i)}, \omega)$, etc. The simultaneous-source responses, defined by equations (22) and (23), become in matrix notation

$$\mathbf{U}^{\text{in}} = \mathbf{G}^{\text{in}}\mathbf{B}, \tag{32}$$

$$\mathbf{U}^{\text{out}} = \mathbf{G}^{\text{out}}\mathbf{B}, \tag{33}$$

where B is the blending matrix. Note that Berkhout (2008) and Mahdad *et al.* (2011) use the symbol Γ to denote the blending matrix, however, to avoid confusion with our point-spread function we denote the blending matrix by **B**. For example, for source groups of two adjacent sources, matrix **B** is defined as follows

$$\mathbf{B} = \begin{pmatrix} a_1 & 0 & \dots & 0 \\ a_2 & 0 & \dots & 0 \\ 0 & a_3 & \dots & 0 \\ 0 & a_4 & \dots & 0 \\ \vdots & \vdots & & \vdots \\ 0 & 0 & \dots & a_{N-1} \\ 0 & 0 & \dots & a_N \end{pmatrix}, \tag{34}$$

where $a_i = \hat{s}^{(i)}(\omega)\exp(-j\omega t_i)$, with $j = \sqrt{-1}$. Multiplying both sides of equation (31) with **B** gives

$$\mathbf{U}^{\text{out}} = \tilde{\mathbf{G}}_{\text{d}}^{\text{out}}\mathbf{U}^{\text{in}}, \tag{35}$$

which is the matrix-equivalent of equation (25).

Suppose there are N sources (before blending) and N receivers, such that the matrices in equation (31) are $N \times N$ matrices. When in the blending process groups are formed of n sources each, then the blending matrix $\mathbf{B}$ is a $N \times (N/n)$ matrix (in equation (34) n equals 2). Matrices $\mathbf{U}^{\text{in}}$ and $\mathbf{U}^{\text{out}}$, defined in equations (32) and (33), are $N \times (N/n)$ matrices. Hence, equation (35), in which matrix $\bar{\mathbf{G}}_{\text{d}}^{\text{out}}$ is the unknown, represents a system of $N \times (N/n)$ equations with $N \times N$ unknowns. Apparently equation (35) is an underdetermined system of equations. However, because the Green's functions in $\bar{\mathbf{G}}_{\text{d}}^{\text{out}}$ are, except close to the source, spatially band-limited (due to the decay of evanescent wavenumber components), equation (35) can be resolved in a band-limited sense, as will be demonstrated below.

In the theory of least-squares inversion there are separate ways for dealing with overdetermined and underdetermined systems (Menke 1989). In the following sections we briefly discuss both approaches.

4.2 Least-squares inversion for overdetermined systems

First we treat equation (35) as an overdetermined system. To obtain its least-squares solution, we multiply both sides of equation (35) with the complex-conjugate transpose of $\mathbf{U}^{\text{in}}$, i.e., with $(\mathbf{U}^{\text{in}})^{\dagger}$. This gives the normal equation (Menke 1989)

$$\mathbf{U}^{\text{out}}(\mathbf{U}^{\text{in}})^{\dagger} = \bar{\mathbf{G}}_{\text{d}}^{\text{out}}\mathbf{U}^{\text{in}}(\mathbf{U}^{\text{in}})^{\dagger}. \tag{36}$$

This is the matrix-equivalent of equation (26) and the basis for least-squares inversion. Analogous to equations (27) and (28) we define the $N \times N$ correlation matrix and point-spread matrix for the simultaneous-source responses as

$$\mathbf{C}_{\text{sim}}^{\text{o}} = \mathbf{U}^{\text{out}}(\mathbf{U}^{\text{in}})^{\dagger} \tag{37}$$

and

$$\Gamma_{\text{sim}}^{\text{o}} = \mathbf{U}^{\text{in}}(\mathbf{U}^{\text{in}})^{\dagger}, \tag{38}$$

respectively, where the superscript "o" stands for "overdetermined". With these definitions, we rewrite equation (36) as

$$C_{\text{sim}}^{\text{o}} = \bar{\mathbf{G}}_{\text{d}}^{\text{out}}\Gamma_{\text{sim}}^{\text{o}}, \tag{39}$$

where $\Gamma_{\text{sim}}^{\text{o}}$ needs to be inverted to resolve $\bar{\mathbf{G}}_{\text{d}}^{\text{out}}$. According to equations (32) and (38) we can write $\Gamma_{\text{sim}}^{\text{o}}$ as

$$\Gamma_{\text{sim}}^{\text{o}} = \mathbf{G}^{\text{in}}\mathbf{B}\mathbf{B}^{\dagger}(\mathbf{G}^{\text{in}})^{\dagger}. \tag{40}$$

Matrix product $\mathbf{B}\mathbf{B}^{\dagger}$ is, for the example in equation (34), given by

$$\mathbf{B}\mathbf{B}^{\dagger} = \begin{pmatrix} |a_1|^2 & a_1a_2^* & 0 & 0 & \dots & 0 & 0 \\ a_2a_1^* & |a_2|^2 & 0 & 0 & \dots & 0 & 0 \\ 0 & 0 & |a_3|^2 & a_3a_4^* & \dots & 0 & 0 \\ 0 & 0 & a_4a_3^* & |a_4|^2 & \dots & 0 & 0 \\ \vdots & \vdots & \vdots & \vdots & \ddots & \vdots & \vdots \\ 0 & 0 & 0 & 0 & \dots & |a_{N-1}|^2 & a_{N-1}a_N^* \\ 0 & 0 & 0 & 0 & \dots & a_Na_{N-1}^* & |a_N|^2 \end{pmatrix}, \tag{41}$$

where the superscript asterisk denotes complex conjugation. Note that the determinant of each of the 2×2 submatrices is zero, hence this matrix is not invertible (this also applies for other forms of the blending matrix $\mathbf{B}$). However, the Green's matrices left and right of $\mathbf{B}\mathbf{B}^{\dagger}$ in equation (40) have a smoothing effect on the sub- and superdiagonals of $\mathbf{B}\mathbf{B}^{\dagger}$. Figures 9a and 9b show the matrix $\Gamma_{\text{sim}}^{\text{o}}$ for a frequency of 23 Hz for the examples of regular and irregular blending, respectively, discussed in section 3.2, i.e, for 32 source groups of four adjacent sources. These figures represent another cross-section of the point-spread functions, already shown in Figures 7c and 8c (that is, Figures 9a,b show $|\hat{\Gamma}_{\text{sim}}^{\text{o}}(\mathbf{x}, \mathbf{x}_A, \omega)|$ for fixed ω, whereas Figures 7c and 8c showed $\Gamma_{\text{sim}}^{\text{o}}(\mathbf{x}, \mathbf{x}_A, t)$ for fixed $\mathbf{x}_A$). Note that the sub- and superdiagonals have indeed been smoothed (i.e., the block structure of equation (41) is no longer present in $\Gamma_{\text{sim}}^{\text{o}}$, shown in Figures 9a and 9b). This makes that matrix $\Gamma_{\text{sim}}^{\text{o}}$ is better invertible, hence $\bar{\mathbf{G}}_{\text{d}}^{\text{out}}$ is resolved from equation (39) via

$$\widehat{\bar{\mathbf{G}}_{\text{d}}^{\text{out}}} = \mathbf{C}_{\text{sim}}^{\text{o}}(\Gamma_{\text{sim}}^{\text{o}} + \epsilon^2\mathbf{I})^{-1}, \tag{42}$$

or

$$\widehat{\bar{\mathbf{G}}_{\text{d}}^{\text{out}}} = \mathbf{U}^{\text{out}}(\mathbf{U}^{\text{in}})^{\dagger}\{\mathbf{U}^{\text{in}}(\mathbf{U}^{\text{in}})^{\dagger} + \epsilon^2\mathbf{I}\}^{-1} \tag{43}$$

(Menke 1989), where $\mathbf{I}$ is the identity matrix, ϵ^2 a stabilization parameter, and the notation $\widehat{\cdot}$ denotes an estimate in the least-squares sense. Note that in principle ϵ^2 can be taken frequency-dependent. However, in all examples in this paper we have chosen a frequency-independent ϵ^2 of $7{*}10^{-6}\,max$, where max is the maximum of the matrix (over all frequencies) to be inverted. Deblending according to equation (43) was illustrated with the examples in Section 3.2.

There are limitations with respect to the conditions under which $\Gamma_{\text{sim}}^{\text{o}}$ can be inverted. For example, for regular blending with eight source groups of sixteen adjacent sources, matrix $\Gamma_{\text{sim}}^{\text{o}}$ is shown in Figure 9c. This matrix is significantly less well conditioned than the one in Figure 9a, meaning that the

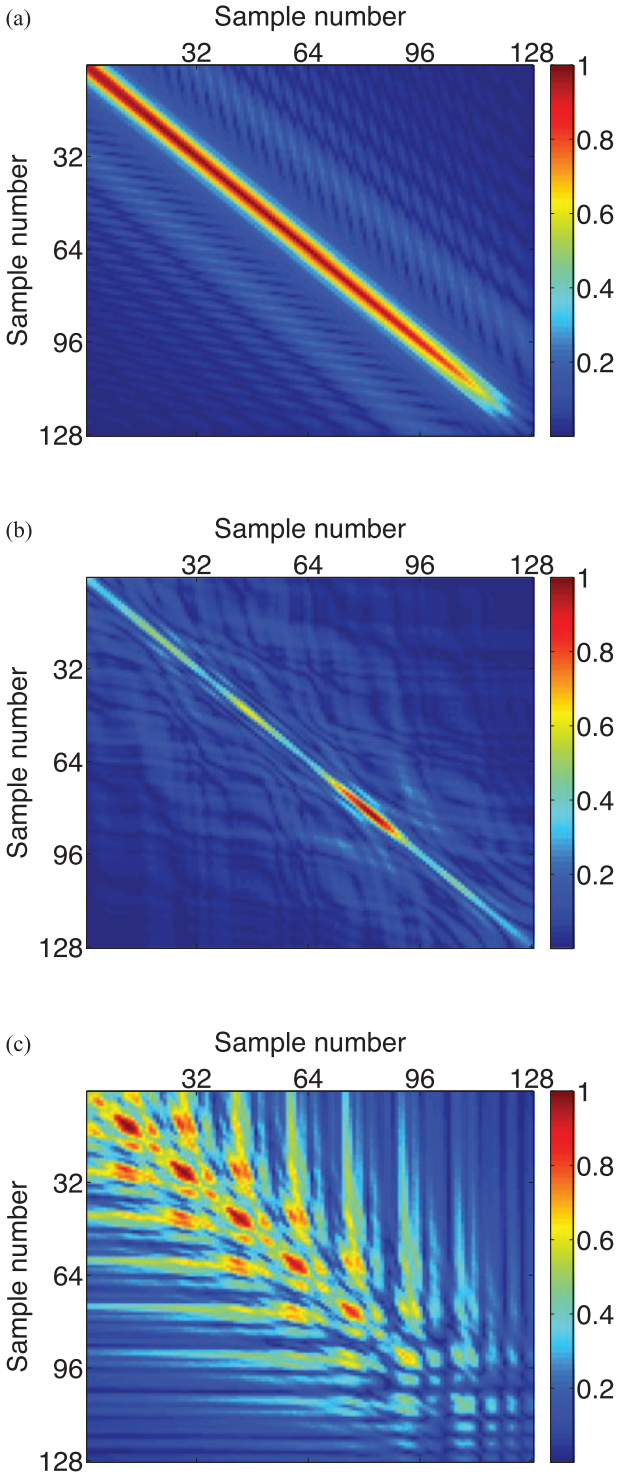

Figure 9 Modulus of matrix $\Gamma^{\mathrm{o}}_{\mathrm{sim}}$ for overdetermined systems for fixed ω. (a) Regular blending with 32 source groups of four adjacent sources. (b) Irregular blending with 32 source groups of four adjacent sources. (c) Regular blending with eight source groups of sixteen adjacent sources.

deblending operation is unstable for this situation. The conditions under which $\Gamma^{\mathrm{o}}_{\mathrm{sim}}$ can be inverted need further investigation, which is beyond the scope of this paper.

4.3 Least-squares inversion for underdetermined systems

Next we treat equation (35) as an underdetermined system (Menke 1989). To this end, we replace equation (43) by

$$\widehat{\bar{G}^{\mathrm{out}}_{\mathrm{d}}} = \mathbf{U}^{\mathrm{out}}\{(\mathbf{U}^{\mathrm{in}})^{\dagger}\mathbf{U}^{\mathrm{in}} + \epsilon^2\mathbf{I}\}^{-1}(\mathbf{U}^{\mathrm{in}})^{\dagger}, \tag{44}$$

or

$$\widehat{\bar{G}^{\mathrm{out}}_{\mathrm{d}}} = \mathbf{U}^{\mathrm{out}}\{\Gamma^{\mathrm{u}}_{\mathrm{sim}} + \epsilon^2\mathbf{I}\}^{-1}(\mathbf{U}^{\mathrm{in}})^{\dagger}, \tag{45}$$

with point-spread matrix $\Gamma^{\mathrm{u}}_{\mathrm{sim}}$ defined as

$$\Gamma^{\mathrm{u}}_{\mathrm{sim}} = (\mathbf{U}^{\mathrm{in}})^{\dagger}\mathbf{U}^{\mathrm{in}}, \tag{46}$$

where superscript "u" stands for "underdetermined". Upon substitution of equation (32) we obtain

$$\Gamma^{\mathrm{u}}_{\mathrm{sim}} = \mathbf{B}^{\dagger}(\mathbf{G}^{\mathrm{in}})^{\dagger}\mathbf{G}^{\mathrm{in}}\mathbf{B}. \tag{47}$$

Note that $N \times N$ matrix $(\mathbf{G}^{\mathrm{in}})^{\dagger}\mathbf{G}^{\mathrm{in}}$ represents an unblended basic point-spread matrix, which we denote as Γ_0, hence

$$\Gamma_0 = (\mathbf{G}^{\mathrm{in}})^{\dagger}\mathbf{G}^{\mathrm{in}}. \tag{48}$$

Matrices $\mathbf{B}^{\dagger}$ and B turn this into an $(N/n) \times (N/n)$ point-spread matrix $\Gamma^{\mathrm{u}}_{\mathrm{sim}}$. We investigate this matrix in more detail for the situation of a homogeneous layer (propagation velocity c) between the acquisition surface and the datum $\mathbb{S}$. Assuming for convenience that the matrix $\mathbf{G}^{\mathrm{in}}$ contains dipole responses, the basic point-spread matrix Γ_0 contains a discretized version of

$$\hat{\Gamma}(x_{1,S}, \omega) = \sin(|\omega|x_{1,S}/c_{\mathrm{a}})/(\pi x_{1,S}), \tag{49}$$

with $c_{\mathrm{a}} = c/\sin\alpha_{\max}$, where $\alpha_{\max}$ is the maximum propagation angle (Wapenaar *et al.*, 2011; Appendix). Hence

$$\Gamma_0 = \begin{pmatrix} \gamma_0 & \gamma_1 & \gamma_2 & \gamma_3 & \cdots & \cdots & & & \\ \gamma_{-1} & \gamma_0 & \gamma_1 & \gamma_2 & \gamma_3 & \cdots & \cdots & & \\ \gamma_{-2} & \gamma_{-1} & \gamma_0 & \gamma_1 & \gamma_2 & \gamma_3 & \cdots & \cdots & \\ \gamma_{-3} & \gamma_{-2} & \gamma_{-1} & \gamma_0 & \gamma_1 & \gamma_2 & \gamma_3 & \cdots & \cdots \\ & \ddots & \ddots & \ddots & \ddots & \ddots & \ddots & \ddots & \\ & & \ddots & \ddots & \ddots & \ddots & \ddots & \ddots & \ddots \end{pmatrix}, \tag{50}$$

with $\gamma_m = \hat{\Gamma}(m\Delta_s, \omega)/\Delta_s$. For the blending matrix B we choose a matrix that creates source groups of two adjacent

sources with a constant time interval, according to

$$\mathrm{B} = \begin{pmatrix} a_1 & 0 & \dots & 0 \\ a_2 & 0 & \dots & 0 \\ 0 & a_1 & \dots & 0 \\ 0 & a_2 & \dots & 0 \\ \vdots & \vdots & & \vdots \\ 0 & 0 & \dots & a_1 \\ 0 & 0 & \dots & a_2 \end{pmatrix}, \tag{51}$$

where $a_i = \hat{s}(\omega)\exp(-j\omega t_i)$. Note that for each of the source groups we have chosen the same parameters a_1 and a_2, which implies that not only the time interval between the sources is constant, but also that each source group has its own time origin (or in other words, the clock is reset for each new source group). In the previous sections we didn't encounter crosstalk between sources in different groups, hence, resetting the time origin would not make any difference. In the matrix product in equation (47), however, crosstalk occurs between the sources in the different groups, so resetting the time origin does make a difference. Upon substitution of equations (50) and (51) into equation (47) we obtain

$$\begin{aligned} \Gamma^{\mathrm{u}}_{\mathrm{sim}} = 2|\hat{s}(\omega)|^2 & \begin{pmatrix} \gamma_0 & \gamma_2 & \gamma_4 & \cdots & \cdots & & \\ \gamma_{-2} & \gamma_0 & \gamma_2 & \gamma_4 & \cdots & \cdots & \\ \gamma_{-4} & \gamma_{-2} & \gamma_0 & \gamma_2 & \gamma_4 & \cdots & \cdots \\ & \ddots & \ddots & \ddots & \ddots & \ddots & \\ & & \ddots & \ddots & \ddots & \ddots & \ddots \end{pmatrix} \\ + |\hat{s}(\omega)|^2\exp(-j\omega\Delta t) & \begin{pmatrix} \gamma_1 & \gamma_3 & \gamma_5 & \cdots & \cdots & & \\ \gamma_{-1} & \gamma_1 & \gamma_3 & \gamma_5 & \cdots & \cdots & \\ \gamma_{-3} & \gamma_{-1} & \gamma_1 & \gamma_3 & \gamma_5 & \cdots & \cdots \\ & \ddots & \ddots & \ddots & \ddots & \ddots & \\ & & \ddots & \ddots & \ddots & \ddots & \ddots \end{pmatrix} \\ + |\hat{s}(\omega)|^2\exp(+j\omega\Delta t) & \begin{pmatrix} \gamma_{-1} & \gamma_1 & \gamma_3 & \cdots & \cdots & & \\ \gamma_{-3} & \gamma_{-1} & \gamma_1 & \gamma_3 & \cdots & \cdots & \\ \gamma_{-5} & \gamma_{-3} & \gamma_{-1} & \gamma_1 & \gamma_3 & \cdots & \cdots \\ & \ddots & \ddots & \ddots & \ddots & \ddots & \\ & & \ddots & \ddots & \ddots & \ddots & \ddots \end{pmatrix}, \end{aligned} \tag{52}$$

with $\Delta t = t_2 - t_1$. The first term on the right-hand side is a resampled version of the basic point-spread matrix Γ_0 of equation (50) (resampling factor 2). The second and third terms are also resampled point-spread matrices, but shifted over a distance $\pm\Delta_s$. Moreover, the factors $\exp(\mp j\omega\Delta t)$ account for a temporal shift $\pm\Delta t$ of the basic point-spread function in the time domain. More generally, if a $N \times (N/n)$ blending matrix B would create source groups of n adjacent sources with regular time intervals, then the $(N/n) \times (N/n)$ point-spread matrix $\Gamma^{\mathrm{u}}_{\mathrm{sim}}$ would be the superposition of (1) one resampled basic point-spread matrix (resampling factor n), multiplied by $n|\hat{s}(\omega)|^2$, (2) two resampled basic point-spread matrices, shifted over a distance $\pm\Delta_s$ and multiplied by $(n-1)|\hat{s}(\omega)|^2\exp(\mp j\omega\Delta t)$, (3) two resampled basic point-spread matrices, shifted over a distance $\pm 2\Delta_s$, multiplied by $(n-2)|\hat{s}(\omega)|^2\exp(\mp 2j\omega\Delta t)$, and so on, until two resampled basic point-spread matrices, shifted over a distance $\pm(n-1)\Delta_s$, multiplied by$|\hat{s}(\omega)|^2\exp(\mp(n-1)j\omega\Delta t)$.

The maximum allowable value of n for unaliased resampling is derived as follows. The resampled point-spread matrices in $\Gamma^{\mathrm{u}}_{\mathrm{sim}}$ contain the basic point-spread function $\hat{\Gamma}(x_{1,S}, \omega)$, sampled with a spatial interval of $n\Delta_s$. This function is sampled unaliased when $n\Delta_s \le \lambda_{\mathrm{a,min}}/2$, where $\lambda_{\mathrm{a,min}}$ is the minimum apparent wavelength covered by the wavenumber spectrum of $\hat{\Gamma}(x_{1,S}, \omega)$. The wavenumber spectrum of $\hat{\Gamma}(x_{1,S}, \omega)$ is constant between $-\omega/c_{\mathrm{a}}$ and ω/c_{a} and zero elsewhere, hence $\lambda_{\mathrm{a,min}} = 2\pi c_{\mathrm{a}}/\omega_{\max} = 2\pi c/(\omega_{\max}\sin\alpha_{\max})$. Hence, $\hat{\Gamma}(x_{1,S}, \omega)$ is sampled unaliased when $n\Delta_s \le \pi c/(\omega_{\max}\sin\alpha_{\max})$.

Figure 10 shows an example for regularly blended data. Figure 10a represents the blended data $u^{\mathrm{out}}(\mathbf{x}_B, \boldsymbol{\sigma}^{(m)}, t)$ for a source group $\boldsymbol{\sigma}^{(m)}$ of four adjacent sources at the center of the acquisition surface. The sources emit transient wavelets, 0.25 s after one another (in total there are 32 source groups). Figure 10b shows the matrix $\Gamma^{\mathrm{u}}_{\mathrm{sim}}$ for a frequency of 23 Hz. This matrix represents $|\hat{\Gamma}^{\mathrm{u}}_{\mathrm{sim}}(\mathbf{x}, \mathbf{x}_A, \omega)|$ for fixed ω. By applying an inverse Fourier transform to $\hat{\Gamma}^{\mathrm{u}}_{\mathrm{sim}}(\mathbf{x}, \mathbf{x}_A, \omega)$ we obtain the space-time domain point-spread function $\Gamma^{\mathrm{u}}_{\mathrm{sim}}(\mathbf{x}, \mathbf{x}_A, t)$. Figure 10c shows this point-spread function for fixed $\mathbf{x}_A$. We apply equation (45) to deblend the data of Figure 10a. The result is shown in Figure 10d. The space-time domain point-spread function as well as the deblended data are hardly distinguishable from those in Figures 7c and 7d, which were obtained with the least-squares approach for overdetermined systems. Note, however, that Figure 7c shows every fourth trace of the point-spread function $\Gamma^{\mathrm{o}}_{\mathrm{sim}}(\mathbf{x}, \mathbf{x}_A, t)$ whereas Figure 10c shows every trace of $\Gamma^{\mathrm{u}}_{\mathrm{sim}}(\mathbf{x}, \mathbf{x}_A, t)$ (both for fixed $\mathbf{x}_A$).

Figure 11 shows a similar example for irregularly blended data. Although the point-spread function $\Gamma^{\mathrm{u}}_{\mathrm{sim}}(\mathbf{x}, \mathbf{x}_A, t)$ in Figure 11c looks very different from $\Gamma^{\mathrm{o}}_{\mathrm{sim}}(\mathbf{x}, \mathbf{x}_A, t)$ in Figure 8c, the deblended result in Figure 11d is hardly distinguishable from that in Figure 8d, which was obtained with the least-squares approach for overdetermined systems.

In these two examples the maximum frequency was 60 Hz and $\alpha_{\max}$ was 78 degrees. Hence, with $c = 2000$ m/s (the

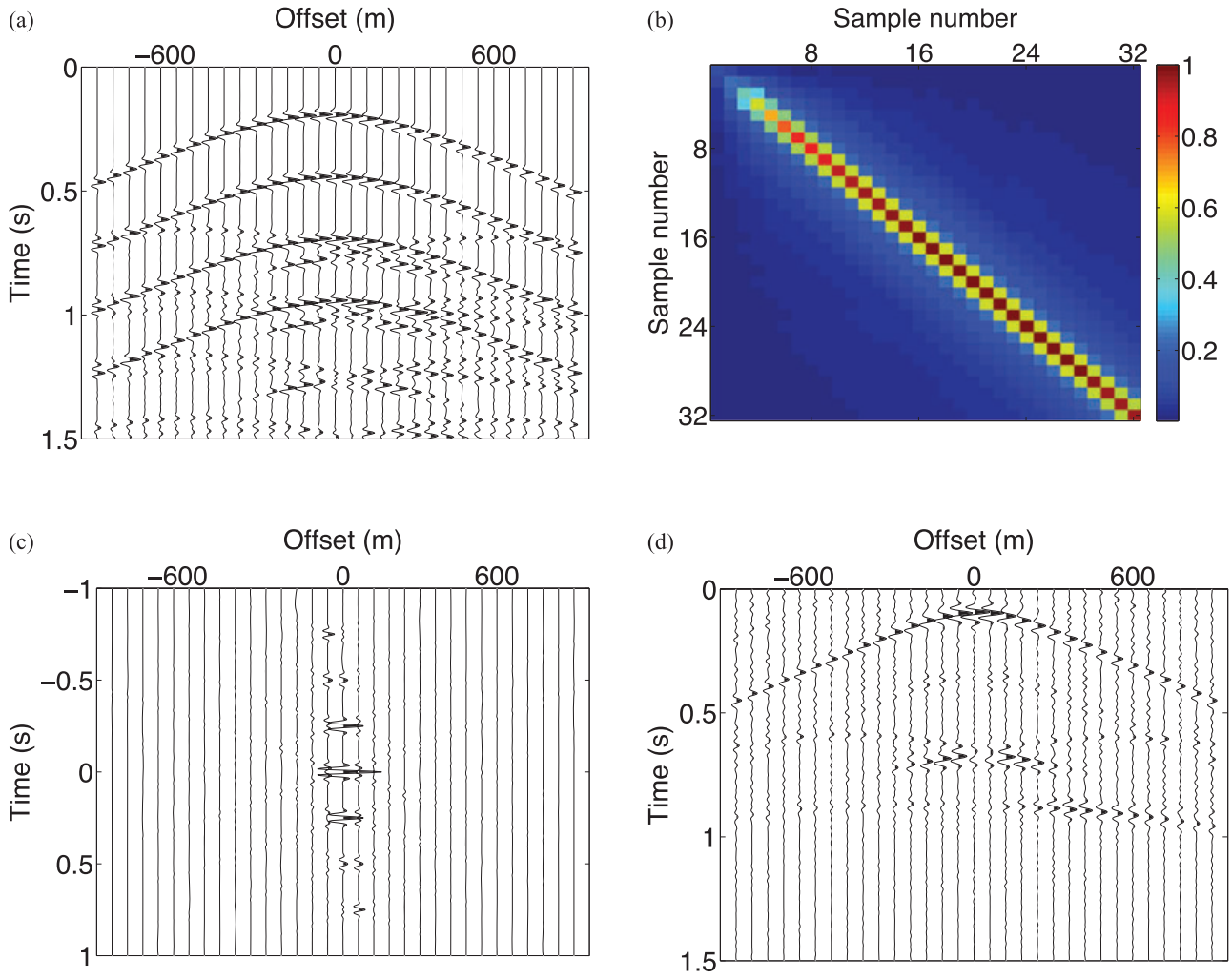

Figure 10 Deblending, using least-squares inversion for underdetermined systems. (a) Regularly blended data $u^{\text{out}}(\mathbf{x}_B, \boldsymbol{\sigma}^{(m)}, t)$ for a source group $\boldsymbol{\sigma}^{(m)}$ of four adjacent sources at the center of the acquisition surface. (b) Modulus of matrix $\Gamma^{\text{u}}_{\text{sim}}$ for fixed ω. (c) Space-time domain point-spread function $\Gamma^{\text{u}}_{\text{sim}}(\mathbf{x}, \mathbf{x}_A, t)$ for fixed $\mathbf{x}_A$. (d) Result of deblending by MDD. (Figures (a) and (d) show every fourth trace; Figure (c) shows every trace.)

velocity of the first layer) we obtain $\lambda_{\text{a,min}}/2 = 17$ m. Since $n\Delta_s = 4 \times 15 = 60$ m, the resampled point-spread matrix is severely aliased. Apparently unaliased resampling of $\Gamma^{\text{u}}_{\text{sim}}(\mathbf{x}, \mathbf{x}_A, t)$ is not a requirement for applying deblending equation (45). The conditions under which equation (45) can be used need further investigation, which is beyond the scope of this paper.

We carry out another experiment, in which we reduce the source interval Δ_s from 15 to 5 m and increase the number of sources per group from 4 to 12 (hence, we keep $n\Delta_s$ equal to 60 m). The receiver spacing remains unchanged (i.e., $\Delta_r = 15$ m). We form 32 groups of 12 adjacent sources, which emit transient wavelets, 0.25 s after one another. Figure 12 shows the results, presented in the same way as the previous two examples. Note that the deblended response in Figure 12d again accurately matches the reference response in Figure 6b. Apparently the deblending method remains valid when the number of sources per group is increased as long as the source interval is decreased at the same rate. This is relevant when the aim of simultaneous-source acquisition is to improve quality (rather than to reduce acquisition time).

5 DEBLENDING BY MULTI-DIMENSIONAL DECONVOLUTION AT THE SURFACE

Because we derived deblending as a form of seismic interferometry by MDD, the resulting deblending algorithms

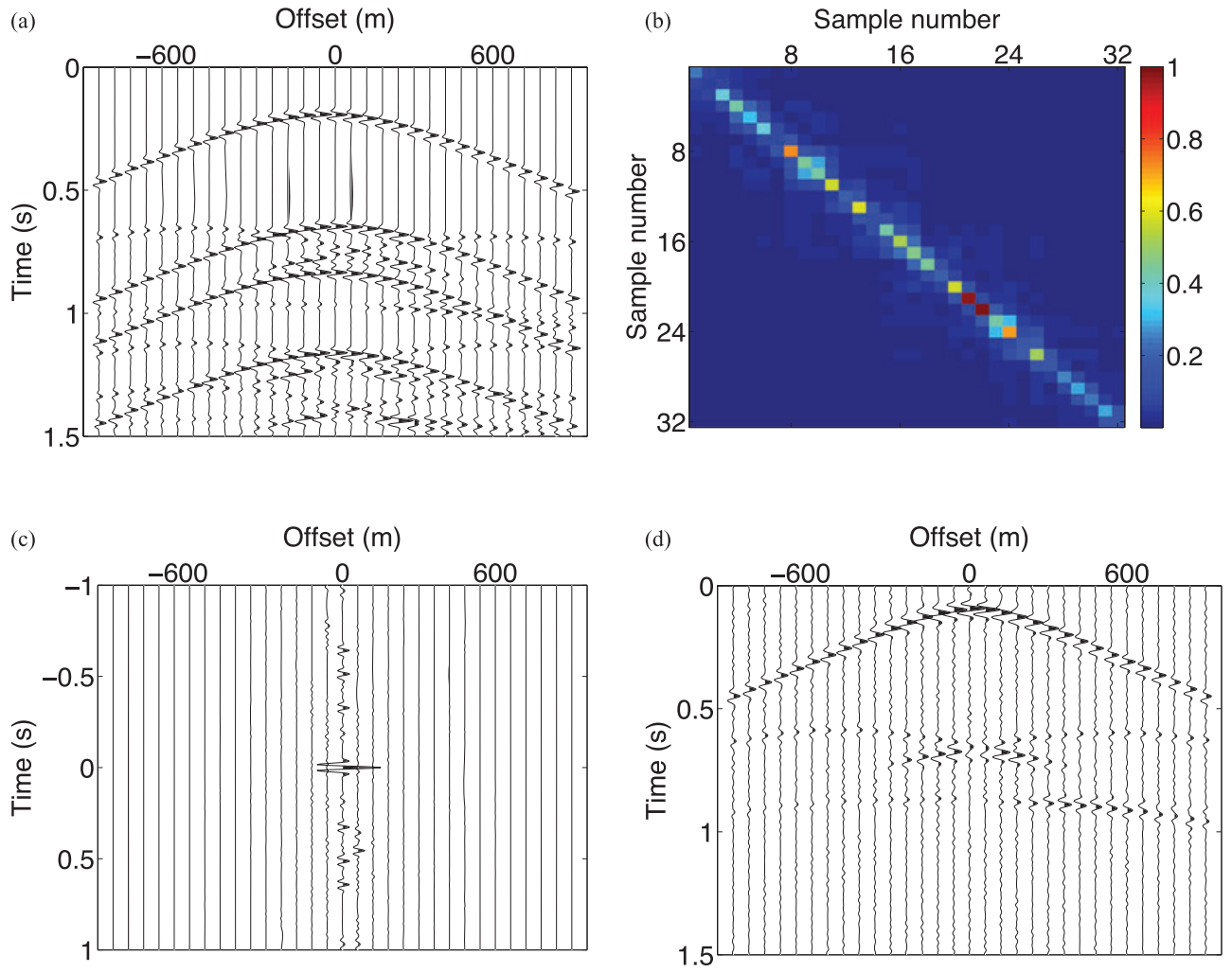

Figure 11 As in Figure 10, but for irregularly blended data (random ignition times).

discussed so far combine the deblending process with data-driven or model-driven redatuming. When the blended wave fields are measured in a borehole, the redatuming step is data-driven. On the other hand, for blended wave fields measured at the surface, the redatuming step is model-driven. For the latter situation the question arises how the discussed methods compare with deblending algorithms that operate directly on blended data at the surface. In the following we briefly review some aspects of an existing method for deblending at the surface, discuss the relation with deblending of redatumed data in the subsurface, and derive in detail an alternative method for deblending by MDD at the surface.

5.1 Review of deblending at the surface

Berkhout (2008) and Mahdad *et al.* (2011) use the following model for blended data at the surface

$$\mathbf{P}_{\mathrm{bl}} = \mathbf{PB}. \tag{53}$$

Here data matrix P contains the unblended data $\hat{P}(\mathbf{x}_R^{(k)}, \mathbf{x}_S^{(i)}, \omega)$ for a given frequency component ω, with sources $\mathbf{x}_S^{(i)}$ and receivers $\mathbf{x}_R^{(k)}$ at the surface. B is the blending matrix (note that we replaced Γ of the aforementioned authors by B, to avoid confusion with our point-spread matrix). $\mathbf{P}_{\mathrm{bl}}$ contains the blended data $\hat{P}_{\mathrm{bl}}(\mathbf{x}_R^{(k)}, \boldsymbol{\sigma}^{(m)}, \omega)$, where $\boldsymbol{\sigma}^{(m)}$ denotes a source group, corresponding to the mth column of blending matrix

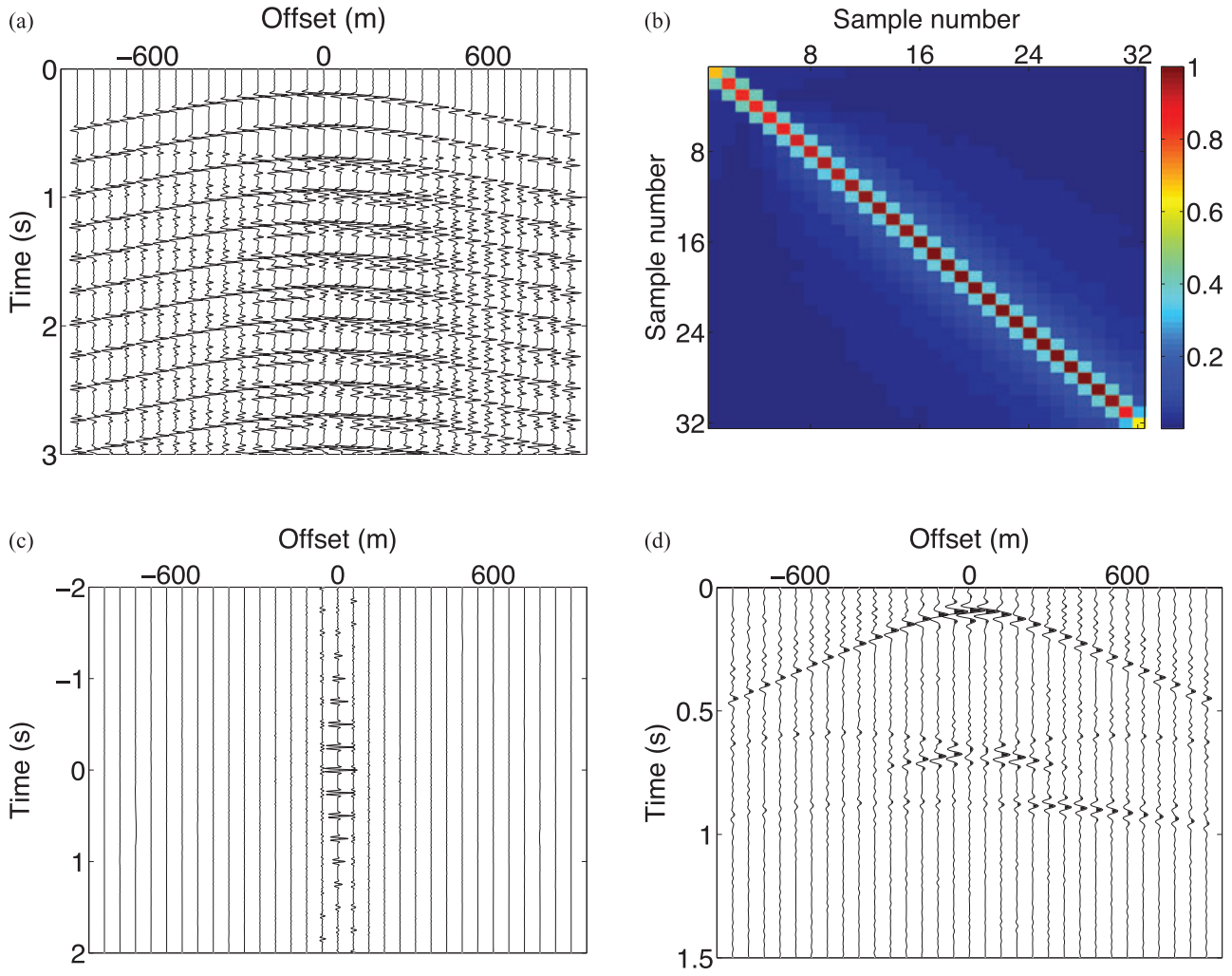

Figure 12 As in Figure 10, but for regularly blended data with 32 source groups of 12 adjacent sources ($\Delta_s = 5$ m).

B. Formally, deblending at the surface is formulated as

$$\widehat{\mathbf{P}} = \mathbf{P}_{\mathrm{bl}}\widehat{\mathbf{B}_{\mathrm{inv}}}, \tag{54}$$

where $\widehat{\mathbf{B}_{\mathrm{inv}}}$ is the inverse of the blending matrix B in some sense. Suppose we would follow a least-squares approach for overdetermined systems, then $\widehat{\mathbf{B}^{\mathrm{o}}_{\mathrm{inv}}}$ would be defined as

$$\widehat{\mathbf{B}^{\mathrm{o}}_{\mathrm{inv}}} = \mathbf{B}^{\dagger}(\mathbf{B}\mathbf{B}^{\dagger} + \epsilon^2\mathbf{I})^{-1}. \tag{55}$$

For the example of matrix B defined in equation (34), the product $\mathbf{B}\mathbf{B}^{\dagger}$ is given in equation (41). This matrix has a zero determinant, which means that the inverse matrix in the right-hand side of equation (55) is fully determined by the stabilization parameter ϵ. Since equation (53) represents an undetermined problem, it is not surprising that equation (55) does not provide a sensible solution.

If we follow the least-squares approach for underdetermined systems, then $\widehat{\mathbf{B}^{\mathrm{u}}_{\mathrm{inv}}}$ is defined as

$$\widehat{\mathbf{B}^{\mathrm{u}}_{\mathrm{inv}}} = (\mathbf{B}^{\dagger}\mathbf{B} + \epsilon^2\mathbf{I})^{-1}\mathbf{B}^{\dagger}. \tag{56}$$

For matrix B defined in equation (34), the product $\mathbf{B}^{\dagger}\mathbf{B}$ is a diagonal matrix, with elements $|\hat{s}^{(1)}(\omega)|^2 + |\hat{s}^{(2)}(\omega)|^2$, $|\hat{s}^{(3)}(\omega)|^2 + |\hat{s}^{(4)}(\omega)|^2$, etc. Other forms of the blending matrix also lead to a diagonal matrix $\mathbf{B}^{\dagger}\mathbf{B}$. When all the source signatures are the same, like in equation (51), we get $\mathbf{B}^{\dagger}\mathbf{B} = 2|\hat{s}(\omega)|^2\mathbf{I}$, i.e., a scaled identity matrix. We conclude that applying $\widehat{\mathbf{B}^{\mathrm{u}}_{\mathrm{inv}}}$ is close to applying $\mathbf{B}^{\dagger}$ only, which is known as pseudo-deblending. This was already observed by Mahdad *et al.* (2011), who proposed instead to resolve P from equation (53) via an iterative procedure.

5.2 Relation with deblending in the subsurface

We now investigate how the deblending algorithms discussed in sections 3 and 4 are related to equations (55) and (56). According to section 3, the response to be resolved is $\bar{G}_{\rm d}^{\rm out}(\mathbf{x}_B, \mathbf{x}, t)$, which has its sources and receivers at datum $\mathbb{S}$ in the subsurface (see Figure 5). In section 4.1 we defined a matrix $\bar{\rm G}_{\rm d}^{\rm out}$, containing $\bar{\hat{G}}_{\rm d}^{\rm out}(\mathbf{x}_B^{(k)}, \mathbf{x}^{(l)}, \omega)$ for a given frequency component ω. In sections 4.2 and 4.3 we denoted the deblended data as $\widehat{\bar{G}_{\rm d}^{\rm out}}$. The sources and receivers of this data matrix, which are situated at datum $\mathbb{S}$, can be redatumed back to the acquisition surface via the following operation (Berkhout 1982; Wapenaar and Berkhout 1989)

$$\widehat{\rm P} = {\rm W}^{-}\widehat{\bar{G}_{\rm d}^{\rm out}}{\rm W}^{+}, \tag{57}$$

where $\rm W^{+}$ and $\rm W^{-}$ represent extrapolation matrices for downgoing and upgoing waves, respectively, and $\widehat{\rm P}$ denotes the deblended data with sources and receivers at the surface. To compare this expression with equations (54) – (56), we substitute either one of the deblending equations (43) or (44) into equation (57). First we substitute equation (43), which is the least-squares approach for overdetermined systems. We thus obtain

$$\widehat{\rm P} = \underbrace{{\rm W}^{-}{\rm U}^{\rm out}}_{\text{blended data}}\ \underbrace{({\rm U}^{\rm in})^{\dagger}\{{\rm U}^{\rm in}({\rm U}^{\rm in})^{\dagger} + \epsilon^2{\rm I}\}^{-1}{\rm W}^{+}}_{\text{deblending operator}}. \tag{58}$$

Since $\rm U^{out}$ contains the blended data $\hat{\boldsymbol{u}}^{\rm out}(\mathbf{x}_B^{(k)}, \boldsymbol{\sigma}^{(m)}, \omega)$, with source groups $\boldsymbol{\sigma}^{(m)}$ at the surface and receivers $\mathbf{x}_B^{(k)}$ at datum plane $\mathbb{S}$ in the subsurface (see Figure 5), the term $\rm W^{-}U^{out}$ represents the blended data with source groups and receivers at the surface. We denote this as $\rm P_{bl}$. The remaining term on the right-hand side is thus the deblending operator at the surface. We denote this as $\widehat{\rm B_{inv}^{o}}$. Hence

$$\widehat{\rm P} = {\rm P_{bl}}\widehat{\rm B_{inv}^{o}}, \tag{59}$$

with

$$\widehat{\rm B_{inv}^{o}} = ({\rm U}^{\rm in})^{\dagger}\{{\rm U}^{\rm in}({\rm U}^{\rm in})^{\dagger} + \epsilon^2{\rm I}\}^{-1}{\rm W}^{+}. \tag{60}$$

Matrix $\rm W^{+}$ contains the responses to dipole sources at the surface. For convenience we replace $\rm W^{+}$ by $\rm G^{in}$, which implies that we assume (like in section 4.3) that $\rm G^{in}$ contains dipole responses. Upon substitution of equation (32) into (60) we thus obtain

$$\widehat{\rm B_{inv}^{o}} = {\rm B}^{\dagger}({\rm G}^{\rm in})^{\dagger}\{{\rm G}^{\rm in}{\rm B}{\rm B}^{\dagger}({\rm G}^{\rm in})^{\dagger} + \epsilon^2{\rm I}\}^{-1}{\rm G}^{\rm in}. \tag{61}$$

Compared with $\widehat{\rm B_{inv}^{o}}$ defined in equation (55), we observe several occurrences of $\rm G^{in}$ and $(\rm G^{in})^{\dagger}$ in equation (61). We noted already in section 4.2 that the matrices $\rm G^{in}$ and $(\rm G^{in})^{\dagger}$ in ${\rm G^{in}BB^{\dagger}(G^{in})^{\dagger}} = \Gamma_{\rm sim}^{\rm o}$ have a smoothing effect on the sub- and superdiagonals of $\rm BB^{\dagger}$, see Figure 9. Hence, unlike equation (55), in which the inverse matrix is unstable, equation (61) contains an inverse that, for moderate deblending problems, is stable.

Next we substitute equation (44), which is the least-squares approach for underdetermined systems, into equation (57). This gives

$$\widehat{\rm P} = \underbrace{{\rm W}^{-}{\rm U}^{\rm out}}_{\text{blended data}}\ \underbrace{\{({\rm U}^{\rm in})^{\dagger}{\rm U}^{\rm in} + \epsilon^2{\rm I}\}^{-1}({\rm U}^{\rm in})^{\dagger}{\rm W}^{+}}_{\text{deblending operator}}, \tag{62}$$

or

$$\widehat{\rm P} = {\rm P_{bl}}\widehat{\rm B_{inv}^{u}}, \tag{63}$$

where

$$\widehat{\rm B_{inv}^{u}} = \{({\rm U}^{\rm in})^{\dagger}{\rm U}^{\rm in} + \epsilon^2{\rm I}\}^{-1}({\rm U}^{\rm in})^{\dagger}{\rm W}^{+}. \tag{64}$$

Replacing $\rm W^{+}$ again by $\rm G^{in}$ and substituting equation (32), yields

$$\widehat{\rm B_{inv}^{u}} = \{{\rm B}^{\dagger}({\rm G}^{\rm in})^{\dagger}{\rm G}^{\rm in}{\rm B} + \epsilon^2{\rm I}\}^{-1}{\rm B}^{\dagger}({\rm G}^{\rm in})^{\dagger}{\rm G}^{\rm in}, \tag{65}$$

or

$$\widehat{\rm B_{inv}^{u}} = \{{\rm B}^{\dagger}\Gamma_0{\rm B} + \epsilon^2{\rm I}\}^{-1}{\rm B}^{\dagger}\Gamma_0, \tag{66}$$

where Γ_0 is the basic point-spread matrix, defined in equation (48). Without this matrix Γ_0, equation (66) would be identical to equation (56). We have seen above that $\rm B^{\dagger}B$ in equation (56) is a diagonal matrix, which implies that $\widehat{\rm B_{inv}^{u}}$, as defined in equation (56), is not much more than a pseudo-deblending operator. On the contrary, ${\rm B}^{\dagger}\Gamma_0{\rm B} = \Gamma_{\rm sim}^{\rm u}$ in equation (66) is a point-spread matrix that consists of a superposition of shifted and resampled versions of the basic point-spread matrix Γ_0, see for example equation (52) and Figures 10 – 12. This makes $\widehat{\rm B_{inv}^{u}}$ as defined in equation (66) a true deblending operator.

5.3 A proposal for deblending by multi-dimensional deconvolution at the surface

Consider the deblending operator $\widehat{\rm B_{inv}^{u}}$ defined in equation (66). Although the basic point-spread matrix Γ_0 is originally defined in terms of Green's matrices, it can be defined directly in terms of the basic point-spread function $\hat{\Gamma}(x_{1,S}, \omega) = \sin(|\omega|x_{1,S}/c_{\rm a})/(\pi x_{1,S})$, with $c_{\rm a} = c/\sin\alpha_{\max}$, see equation (50) for details. Hence, instead of combining deblending with redatuming, as discussed in section 4.3, one can construct the deblending operator $\widehat{\rm B_{inv}^{u}}$, as defined in equation (66), from the blending matrix B and the basic

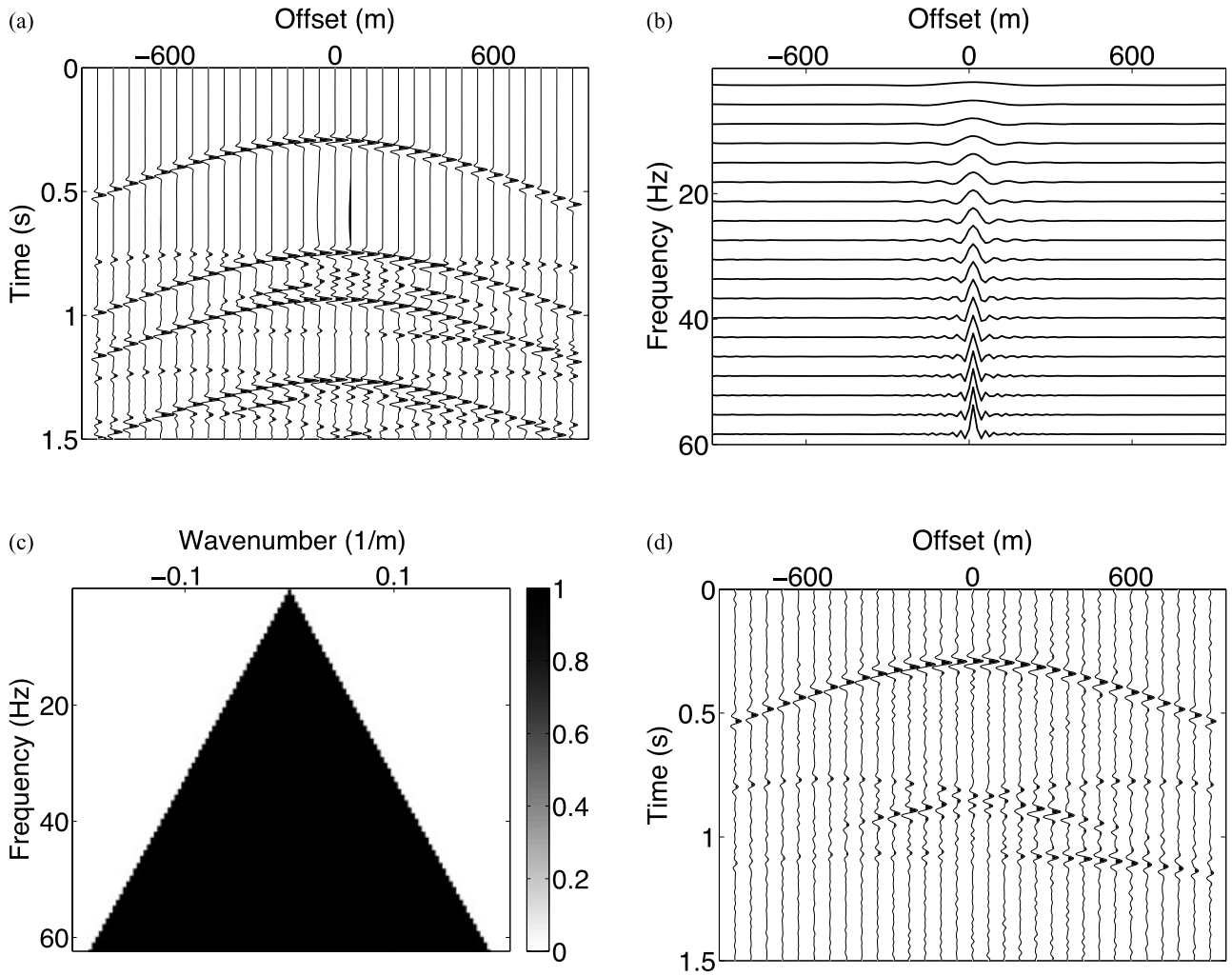

Figure 13 Example of deblending by MDD at the surface. (a) Irregularly blended data for a source group at the center of the acquisition surface, observed by receivers at the surface. (b) The basic point-spread function $\hat{\Gamma}(x_{1,S}, \omega)$. (c) Fourier transform of figure (b). This is a filter that passes propagating waves up to an angle of 78 degrees. (d) Deblended data at the surface. (Figures (a) and (d) show every fourth trace).

point-spread function $\hat{\Gamma}(x_{1,S}, \omega)$, and apply this operator directly to the blended data at the surface, according to equation (63). The effect of the point-spread matrix Γ_0 is two-fold: (1) the inverse of $B^{\dagger}\Gamma_0 B$ in equation (66) takes care of the actual deblending, and (2) the matrix Γ_0 at the far right in equation (66) suppresses the wavenumber components for which the inverse matrix is unstable. These suppressed wavenumber components correspond to evanescent waves and waves propagating beyond $\alpha_{\max}$, i.e, wavenumber components that are not present in the blended data anyway. Note that, although we avoid the redatuming step in this way, we still need some information about the shallow subsurface, namely the propagation velocity and the maximum propagation angle, to construct the basic point-spread function $\hat{\Gamma}(x_{1,S}, \omega)$. However, because sources and receivers stay at the surface, this method is less sensitive to the used velocity than the combined deblending and redatuming method discussed in section 4.3.

We illustrate this method with a numerical example. We consider again the configuration of Figure 6a, this time with sources and receivers at the surface, with $\Delta_s = \Delta_r = 15$ m. We form 32 groups of four adjacent sources with random ignition times between 0 and 1 s. Figure 13a shows the blended data for a source group at the center of the surface. After a temporal Fourier transform, the blended data for different source groups represent the columns of matrix P_{bl}. Figure 13b shows the basic point-spread function $\hat{\Gamma}(x_{1,S}, \omega)$, as defined in equation (49) with $c = 2000$ m/s and $\alpha_{\max} = 78$ degrees, for a range of frequencies. Figure 13c is the spatial Fourier

transform of $\hat{\Gamma}(x_{1,S}, \omega)$. This is a filter that passes propagating waves up to an angle of 78 degrees and suppresses waves with larger angles as well as evanescent waves. The Nyquist wavenumbers are $\pm\pi/\Delta_s$, with $\Delta_s = 15$ m. We define the samples of the point-spread function as $\gamma_m = \hat{\Gamma}(m\Delta_s, \omega)/\Delta_s$ and construct the basic point-spread matrix Γ_0 according to equation (50). With this, we construct the point-spread matrix for the blended data $\Gamma^{\mathrm{u}}_{\mathrm{sim}} = \mathrm{B}^{\dagger}\Gamma_0\mathrm{B}$ and, using equation (66), the deblending operator $\widehat{\mathrm{B}^{\mathrm{u}}_{\mathrm{inv}}}$. We apply this matrix to the blended data matrix P_{bl}, according to equation (63), and thus obtain the deblended data $\widehat{\mathrm{P}}$. After an inverse temporal Fourier transform, we obtain the deblended surface data in the space-time domain, see Figure 13d. Note that this deblending result is comparable with that in Figure 11d, except that the response in Figure 13d has its source and receivers at the acquisition surface.

6 CONCLUSIONS

We have shown that there is a close relationship between seismic interferometry and the simultaneous-source method. In seismic interferometry, new responses are formed from existing responses at different receivers. Of course no new information is created, but information hidden in noise or in a complex scattering coda is unravelled and reorganized into easily interpretable responses. Seismic interferometry can be applied to sequential controlled-source responses or to ambient noise coming from simultaneous noise sources.

In the simultaneous-source method, responses to small groups of sources are measured with overlap. This type of acquisition is intermediate between the two types of acquisition underlying seismic interferometry. Hence, with some modifications, seismic interferometry can unravel simultaneous-source data and reorganize it into sequential source responses. Another name for simultaneous-source acquisition is blended acquisition, hence, the unravelling process is also called deblending.

Seismic interferometry can be applied as a trace-by-trace crosscorrelation process or as a multidimensional deconvolution (MDD) process. The crosscorrelation approach applied to blended data is equivalent with pseudo-deblending, i.e., events are moved to the correct position and traveltime, but the crosstalk between different sources is not removed. On the other hand, deblending by MDD moves events to the correct position and suppresses the crosstalk. A point-spread function, defined in a similar way as for seismic interferometry by MDD, explains the crosstalk in the correlation function. Hence, the inverse point-spread function removes the crosstalk from the correlation function and thus turns pseudo-deblended data into truly deblended data.

Seismic interferometry by MDD, and hence deblending by MDD, are essentially least-squares inversion problems. At first sight the deblending problem seems underdetermined, however, because the response to be resolved is spatially band-limited, it appears that under specific circumstances a stable least-squares inversion is possible. We have compared approaches for overdetermined and underdetermined systems. For the considered examples, both approaches give similar results. The approach for underdetermined systems inverts smaller matrices and is therefore computationally more efficient. However, it needs further research before we can conclude which of the two approaches is to be preferred in general. Another aspect that needs further investigation is the type of regularization to stabilize the matrix inversion. We used a simple Tikhonov regularization which worked well for the considered examples, but more advanced regularizations may give further improvements in more complex situations.

Unlike iterative deblending procedures discussed in the literature, deblending by MDD is implemented as a direct matrix inversion, which is significantly more efficient. Moreover, it does not make assumptions about incoherency or sparsity of the blending noise (i.e., the crosstalk). Nevertheless, irregular ignition times are advantageous because they reduce the notches in the spectrum of the point-spread function and hence improve the stability of the inversion. The sources that are combined per source group are preferably located close to each other, so that the matrix to be inverted (i.e., the point-spread matrix) has a narrow band structure. The number of sources that can be taken together per group is limited, but can be increased by reducing the spatial source interval. This is relevant when the aim of simultaneous-source acquisition is to improve quality.

Because we derived deblending by MDD as a form of seismic interferometry, the proposed procedure combines deblending with redatuming. However, we showed that the method can be easily turned into an algorithm for deblending at the acquisition surface. An essential element in the resulting scheme is again that a direct inversion of the point-spread matrix suppresses the crosstalk in the blended data.

ACKNOWLEDGEMENTS

This work is supported by the Netherlands Research Centre for Integrated Solid Earth Science (ISES) and the Dutch Technology Foundation STW (grant DCB.7913). We thank Ivan

Vasconcelos, three anonymous reviewers and the associate editor (Claudio Bagaini) for their constructive comments, which helped us to improve the paper.

REFERENCES

Abma R. L., Manning T., Tanis M., Yu J. and Foster M., 2010. High quality separation of simultaneous sources by sparse inversion, in *EAGE, Extended Abstracts*, B003.

Akerberg P., Hampson G., Rickett J., Martin H. and Cole J., 2008. Simultaneous source separation by sparse Radon transform, in *SEG, Expanded Abstracts*, pp. 2801–2805.

Bagaini C., 2006. Overview of simultaneous Vibroseis acquisition methods, in *SEG, Expanded Abstracts*, pp. 70–74.

Bakulin A. and Calvert R., 2004. Virtual source: new method for imaging and 4D below complex overburden, in *SEG, Expanded Abstracts*, pp. 2477–2480.

Bakulin A. and Calvert R., 2006. The virtual source method: Theory and case study, *Geophysics*, **71**(4), SI139–SI150.

Beasley C. J., 2008. A new look at marine simultaneous sources, *The Leading Edge*, **27**(7), 914–917.

Beasley C. J., Chambers R. E. and Jiang Z., 1998. A new look at simultaneous sources, in *SEG, Expanded Abstracts*, pp. 133–135.

Berkhout A. J., 1982. *Seismic Migration. Imaging of acoustic energy by wave field extrapolation*, Elsevier.

Berkhout A. J., 2008. Changing the mindset in seismic data acquisition, *The Leading Edge*, **27**(7), 924–938.

Dai W. and Schuster J., 2009. Least-squares migration of simultaneous sources data with a deblurring filter, in *SEG, Expanded Abstracts*, pp. 2990–2994.

de Hoop M. V., Garnier J., Holman S. F. and Sølna K., 2012. Retrieval of a Green's function with reflections from partly coherent waves generated by a wave packet using cross correlations, *SIAM J. Appl. Math.*, (submitted).

Draganov D., Wapenaar K., Mulder W., Singer J. and Verdel A., 2007. Retrieval of reflections from seismic background-noise measurements, *Geophysical Research Letters*, **34**, L04305.

Gouédard P., Stehly L., Brenguier F., Campillo M., Colin de Verdière Y., Larose E., Margerin L., Roux P., Sánchez-Sesma F. J., Shapiro N. M. and Weaver R. L., 2008. Cross-correlation of random fields: mathematical approach and applications, *Geophysical Prospecting*, **56**, 375–393.

Hampson G., Stefani J. and Herkenhoff F., 2008. Acquisition using simultaneous sources, *The Leading Edge*, **27**(7), 918–923.

Herrmann F. J., Erlangga Y. A. and Lin T. T. Y., 2009. Compressive simultaneous full-waveform simulation, *Geophysics*, **74**(4), A35–A40.

Howe D., Foster M., Allen T., Taylor B. and Jack I., 2008. Independent simultaneous sweeping - a method to increase the productivity of land seismic crews, in *SEG, Expanded Abstracts*, pp. 2826–2830.

Huo S., Luo Y. and Kelamis P., 2009. Simultaneous sources separation via multi-directional vector-median filter, in *SEG, Expanded Abstracts*, pp. 31–35.

Ikelle L., 2007. Coding and decoding: seismic data modeling, acquisition and processing, in *SEG, Expanded Abstracts*, pp. 66–70.

Kim Y., Gruzinov I., Guo M. and Sen S., 2009. Source separation of simultaneous source OBC data, in *SEG, Expanded Abstracts*, pp. 51–55.

Larose E., Margerin L., Derode A., van Tiggelen B., Campillo M., Shapiro N., Paul A., Stehly L. and Tanter M., 2006. Correlation of random wave fields: An interdisciplinary review, *Geophysics*, **71**(4), SI11–SI21.

Mahdad A., Doulgeris P. and Blacquière G., 2011. Separation of blended data by iterative estimation and subtraction of blending interference noise, *Geophysics*, **76**(3), Q9–Q17.

Mehta K., Bakulin A., Sheiman J., Calvert R. and Snieder R., 2007. Improving the virtual source method by wavefield separation, *Geophysics*, **72**(4), V79–V86.

Menke W., 1989. *Geophysical data analysis*, Academic Press.

Moore I., Dragoset B., Ommundsen T., Wilson D., Ward C. and Eke D., 2008. Simultaneous source separation using dithered sources, in *SEG, Expanded Abstracts*, pp. 2806–2810.

Neelamani R., Krohn C. E., Krebs J. R., Deffenbaugh M., Anderson J. E. and Romberg J. K., 2008. Efficient seismic forward modeling using simultaneous random sources and sparsity, in *SEG, Expanded Abstracts*, pp. 2107–2111.

Romero L. A., Ghiglia D. C., Ober C. C. and Morton S. A., 2000. Phase encoding of shot records in prestack migration, *Geophysics*, **65**(2), 426–436.

Schuster G. T. and Zhou M., 2006. A theoretical overview of model-based and correlation-based redatuming methods, *Geophysics*, **71**(4), SI103–SI110.

Schuster G. T., Yu J., Sheng J. and Rickett J., 2004. Interferometric/daylight seismic imaging, *Geophysical Journal International*, **157**, 838–852.

Schuster G. T., Wang X., Huang Y., Dai W. and Boonyasiriwat C., 2011. Theory of multisource crosstalk reduction by phase-encoded statics, *Geophysical Journal International*, **184**, 1289–1303.

Shapiro N. M. and Campillo M., 2004. Emergence of broadband Rayleigh waves from correlations of the ambient seismic noise, *Geophysical Research Letters*, **31**, L07614.

Spitz S., Hampson G. and Pica A., 2008. Simultaneous source separation: a prediction-subtraction approach, in *SEG, Expanded Abstracts*, pp. 2811–2815.

Stefani J., Hampson G. and Herkenhoff E. F., 2007. Acquisition using simultaneous sources, in *EAGE, Extended Abstracts*, B006.

Tang Y. and Biondi B., 2009. Least-squares migration/inversion of blended data, in *SEG, Expanded Abstracts*, pp. 2859–2863.

van der Neut J., Ruigrok E., Draganov D. and Wapenaar K., 2010. Retrieving the earth's reflection response by multi-dimensional deconvolution of ambient seismic noise, in *EAGE, Extended Abstracts*, P406.

van der Neut J., Thorbecke J., Mehta K., Slob E. and Wapenaar K., 2011. Controlled-source interferometric redatuming by cross-correlation and multidimensional deconvolution in elastic media, *Geophysics*, **76**(4), SA63–SA76.

Verschuur D. J. and Berkhout A. J., 2011. Seismic migration of blended shot records with surface-related multiple scattering, *Geophysics*, **76**(1), A7–A13.

Wapenaar C. P. A. and Berkhout A. J., 1989. *Elastic wave field extrapolation*, Elsevier, Amsterdam.

Wapenaar K., Slob E. and Snieder R., 2008. Seismic and electromagnetic controlled-source interferometry in dissipative media, *Geophysical Prospecting*, **56**, 419–434.

Wapenaar K., van der Neut J., Ruigrok E., Draganov D., Hunziker J., Slob E., Thorbecke J. and Snieder R., 2011. Seismic interferometry by crosscorrelation and by multidimensional deconvolution: a systematic comparison, *Geophysical Journal International*, **185**, 1335–1364.

APPENDIX A: COMPARISON OF THE CORRELATION AND POINT-SPREAD FUNCTIONS

Equations (11), (19) and (29) have identical forms. Each of these equations states that the correlation function is proportional to the sought Green's function, with its source smeared in space and time by the point-spread function. In equation (11) the correlation function and the point-spread function are obtained from responses to sequential transient sources, in equation (19) from responses to simultaneous noise sources and in equation (29) from responses to simultaneous transient sources. Here we compare the correlation and point-spread functions for these three situations in more detail.

Substituting the expressions for the responses to sequential transient sources (equations (4) and (5)) into equations (9) and (10), using equation (6), gives the following results for the correlation and point-spread function for sequential transient sources

$$C_{\rm seq}(\mathbf{x}_B, \mathbf{x}_A, t) = \sum_i G^{\rm out}(\mathbf{x}_B, \mathbf{x}_S^{(i)}, t) * G^{\rm in}(\mathbf{x}_A, \mathbf{x}_S^{(i)}, -t) * S_{\rm seq}^{(i)}(t), \tag{A1}$$

$$\Gamma_{\rm seq}(\mathbf{x}, \mathbf{x}_A, t) = \sum_i G^{\rm in}(\mathbf{x}, \mathbf{x}_S^{(i)}, t) * G^{\rm in}(\mathbf{x}_A, \mathbf{x}_S^{(i)}, -t) * S_{\rm seq}^{(i)}(t). \tag{A2}$$

Similarly, substituting equations (12) and (13) into equations (17) and (18), using equation (14), yields the following expressions for the correlation and point-spread function for simultaneous noise sources

$$C_{\rm noise}(\mathbf{x}_B, \mathbf{x}_A, t) = \sum_i \sum_j G^{\rm out}(\mathbf{x}_B, \mathbf{x}_S^{(i)}, t) * G^{\rm in}(\mathbf{x}_A, \mathbf{x}_S^{(j)}, -t) * S_{\rm noise}^{(ij)}(t), \tag{A3}$$

$$\Gamma_{\rm noise}(\mathbf{x}, \mathbf{x}_A, t) = \sum_i \sum_j G^{\rm in}(\mathbf{x}, \mathbf{x}_S^{(i)}, t) * G^{\rm in}(\mathbf{x}_A, \mathbf{x}_S^{(j)}, -t) * S_{\rm noise}^{(ij)}(t). \tag{A4}$$

For the special case that the noise sources are mutually uncorrelated, according to

$$\langle N^{(i)}(t) * N^{(j)}(-t) \rangle = S_{\rm noise}^{(ij)}(t) = \delta_{ij} S_{\rm noise}^{(i)}(t), \tag{A5}$$

where $S_{\rm noise}^{(i)}(t)$ is the autocorrelation of the ith noise source, equations (A3) and (A4) become

$$C_{\rm noise}(\mathbf{x}_B, \mathbf{x}_A, t) = \sum_i G^{\rm out}(\mathbf{x}_B, \mathbf{x}_S^{(i)}, t) * G^{\rm in}(\mathbf{x}_A, \mathbf{x}_S^{(i)}, -t) * S_{\rm noise}^{(i)}(t), \tag{A6}$$

$$\Gamma_{\rm noise}(\mathbf{x}, \mathbf{x}_A, t) = \sum_i G^{\rm in}(\mathbf{x}, \mathbf{x}_S^{(i)}, t) * G^{\rm in}(\mathbf{x}_A, \mathbf{x}_S^{(i)}, -t) * S_{\rm noise}^{(i)}(t). \tag{A7}$$

Note that these expressions are identical to those for sequential transient sources (equations (A1) and (A2)), with the autocorrelations of the sequential transient signals, $S_{\rm seq}^{(i)}(t)$, replaced by the autocorrelations of the noise sources, $S_{\rm noise}^{(i)}(t)$.

Next, substituting the expressions for the simultaneous-source responses (equations (22) and (23)) into equations (27) and (28), using equation (24), gives

$$\begin{aligned} C_{\rm sim}(\mathbf{x}_B, \mathbf{x}_A, t) &= \sum_m \sum_{\{\mathbf{x}_S^{(i)}, \mathbf{x}_S^{(j)}\} \in \sigma^{(m)}} G^{\rm out}(\mathbf{x}_B, \mathbf{x}_S^{(i)}, t) * G^{\rm in}(\mathbf{x}_A, \mathbf{x}_S^{(j)}, -t) * S_{\rm sim}^{(ij)}(t - t_i + t_j) \\ &= \sum_m \sum_{\mathbf{x}_S^{(i)} \in \sigma^{(m)}} G^{\rm out}(\mathbf{x}_B, \mathbf{x}_S^{(i)}, t) * G^{\rm in}(\mathbf{x}_A, \mathbf{x}_S^{(i)}, -t) * S_{\rm sim}^{(ii)}(t) \\ &\quad + \sum_m \sum_{\{\mathbf{x}_S^{(i)}, \mathbf{x}_S^{(j)}\} \in \sigma^{(m)}, i \neq j} G^{\rm out}(\mathbf{x}_B, \mathbf{x}_S^{(i)}, t) * G^{\rm in}(\mathbf{x}_A, \mathbf{x}_S^{(j)}, -t) * S_{\rm sim}^{(ij)}(t - t_i + t_j) \end{aligned} \tag{A8}$$

and

$$\begin{aligned} \Gamma_{\rm sim}(\mathbf{x}, \mathbf{x}_A, t) &= \sum_m \sum_{\{\mathbf{x}_S^{(i)}, \mathbf{x}_S^{(j)}\} \in \sigma^{(m)}} G^{\rm in}(\mathbf{x}, \mathbf{x}_S^{(i)}, t) * G^{\rm in}(\mathbf{x}_A, \mathbf{x}_S^{(j)}, -t) * S_{\rm sim}^{(ij)}(t - t_i + t_j) \\ &= \sum_m \sum_{\mathbf{x}_S^{(i)} \in \sigma^{(m)}} G^{\rm in}(\mathbf{x}, \mathbf{x}_S^{(i)}, t) * G^{\rm in}(\mathbf{x}_A, \mathbf{x}_S^{(i)}, -t) * S_{\rm sim}^{(ii)}(t) \\ &\quad + \sum_m \sum_{\{\mathbf{x}_S^{(i)}, \mathbf{x}_S^{(j)}\} \in \sigma^{(m)}, i \neq j} G^{\rm in}(\mathbf{x}, \mathbf{x}_S^{(i)}, t) * G^{\rm in}(\mathbf{x}_A, \mathbf{x}_S^{(j)}, -t) * S_{\rm sim}^{(ij)}(t - t_i + t_j), \end{aligned} \tag{A9}$$

or

$$C_{\rm sim}(\mathbf{x}_B, \mathbf{x}_A, t) = \sum_i G^{\rm out}(\mathbf{x}_B, \mathbf{x}_S^{(i)}, t) * G^{\rm in}(\mathbf{x}_A, \mathbf{x}_S^{(i)}, -t) * S_{\rm sim}^{(ii)}(t) + \text{“crosstalk”} \tag{A10}$$

and

$$\Gamma_{\mathrm{sim}}(\mathbf{x}, \mathbf{x}_A, t) = \sum_i G^{\mathrm{in}}(\mathbf{x}, \mathbf{x}_S^{(i)}, t) * G^{\mathrm{in}}(\mathbf{x}_A, \mathbf{x}_S^{(i)}, -t) * S_{\mathrm{sim}}^{(ii)}(t) + \text{“crosstalk”}. \quad \text{(A11)}$$

The expressions for sequential transient sources as well as those for simultaneous noise sources can be obtained as limiting cases. When each source group $\boldsymbol{\sigma}^{(m)}$ contains one source only and $S_{\mathrm{sim}}^{(ii)}(t) = S_{\mathrm{seq}}^{(i)}(t)$, equations (A8) and (A9) reduce to the expressions for sequential transient sources, equations (A1) and (A2), respectively. On the other hand, when there is only one source group containing all sources and when the source wavelets with crosscorrelation $S_{\mathrm{sim}}^{(ij)}(t - t_i + t_j)$ are replaced by noise signals with crosscorrelation $S_{\mathrm{noise}}^{(ij)}(t)$, then we obtain the expressions for simultaneous noise sources, equations (A3) and (A4). We have already seen that the latter equations further reduce to equations (A6) and (A7) when the noise sources are mutually uncorrelated, i.e., when $S_{\mathrm{noise}}^{(ij)}(t) = \delta_{ij} S_{\mathrm{noise}}^{(i)}(t)$.